

ON THE INFLUENCE OF THE GEOMETRY ON SKIN EFFECT IN ELECTROMAGNETISM

GABRIEL CALOZ, MONIQUE DAUGE, ERWAN FAOU, VICTOR PÉRON

ABSTRACT. We consider the equations of electromagnetism set on a domain made of a dielectric and a conductor subdomain in a regime where the conductivity is large. Assuming smoothness for the dielectric–conductor interface, relying on recent works we prove that the solution of the Maxwell equations admits a multiscale asymptotic expansion with profile terms rapidly decaying inside the conductor. This *skin effect* is measured by introducing a skin depth function that turns out to depend on the mean curvature of the boundary of the conductor. We then confirm these asymptotic results by numerical experiments in various axisymmetric configurations. We also investigate numerically the case of a nonsmooth interface, namely a cylindrical conductor.

CONTENTS

1. Introduction	1
2. Framework	3
3. Multiscale expansion	5
4. Axisymmetric domains	7
5. Finite element discretizations and computations	13
6. Numerical simulations of skin effect	17
7. Postprocessing	21
8. Conclusion	25
Appendix A. Elements of proof for the multiscale expansion	25
Appendix B. The multiscale expansion of the orthoradial component	33
References	36

1. INTRODUCTION

Our interest lies in the influence of the geometry of a conducting body on the skin effect in electromagnetism. This effect describes the rapid decay of electromagnetic fields with depth inside a metallic conductor. The skin effect reflects the flow of current near the surface of a conductor. After the early work [18], the mathematical analysis of the skin effect has been addressed more recently in several papers, [20, 11, 12, 8].

The present work is motivated by recent studies [8, 4, 3, 17] in which authors analyze the behavior of the electromagnetic fields solution of the Maxwell equations through an asymptotic expansion for large conductivity. In particular, uniform estimates for the

electromagnetic field at high conductivity are proved in [3], whereas in the note [4] a suitable skin depth function is introduced on the interface between a conductor and an insulator to generalize the classical scalar quantity. An asymptotic expansion at high conductivity for this function shows the influence of the geometry of the interface : the skin depth is larger for high conductivity when the mean curvature of the conducting body surface is larger – and here the sign of the curvature has a major influence, which means that the skin depth is larger in convex than in concave conductors.

In this paper, our aim is twofold

- (1) Present elements of derivation for asymptotic expansions near the conductor-insulator interface,
- (2) Illustrate by numerical computations the theoretical behavior deduced from asymptotic analysis in [4].

For our computations, we consider a special class of axisymmetric problems, which allows their reduction to two-dimensional scalar problems. This enables to measure the skin effect with reduced computational effort. We perform finite element computations for relevant benchmarks (cylinders and spheroids). The interface problem for the magnetic field is solved with the library Mélima [13]. A postprocessing shows the accuracy of the asymptotic expansion, and exhibits the influence of the mean curvature of the conductor on the skin effect. Our computations also clearly display the effect of the edges of the cylindrical conductor: In this case, the decay is not exponential near edges while becoming exponential further away from edges.

The presentation of the paper proceeds as follows. In section 2, we introduce the framework: we present the Maxwell equations and the result of [3] about existence of solution at high conductivity and the formulation for the magnetic field. In section 3, we present the asymptotic expansion of the magnetic field in the smooth case, and the asymptotic behavior of the skin depth for high conductivity. In section 4, we restrict our considerations to axisymmetric domains and orthoradial axisymmetric data, and we present the configurations A (cylindrical), B, and C (spheroidal), chosen for computations. In section 5, we introduce a finite element discretization for the solution of the problem in the meridian domain, and we check the convergence of the discretized problem. In section 6, we present numerical simulations in all configurations to highlight the skin effect, and to exhibit the influence of the mean curvature of the conductor on the skin effect. In section 7, we perform post-treatments of our numerical computations in configurations A (cylindrical) and B (spheroidal) in order to investigate the nature of the decay of the field inside the conductor: In smooth configurations (B) the rate of the exponential decay is very close to the expected theoretical one, while in corner configurations (A) the exponential decay shows up in a region which is not very close to the corner. Theoretical aspects in this latter case are going to be studied in [5]. In Appendix A, we provide elements of proof for the multiscale expansion given in section 3. We expand the Maxwell operators in power series, and we obtain the equations satisfied by

the magnetic and electric profiles. In Appendix B, we derive the profiles of the ortho-radial component of the magnetic field in relation with the 3D asymptotic expansion in axisymmetric configurations.

2. FRAMEWORK

Let Ω be a piecewise smooth Lipschitz domain. We denote by Γ its boundary and by \mathbf{n} the outer unit normal field on Γ . We denote by $\mathbf{L}^2(\Omega)$ the space of three-component fields square integrable on Ω .

We consider the Maxwell equations given by Faraday's and Ampère's laws in Ω :

$$(2.1) \quad \text{curl } \mathbf{E} - i\omega\mu_0 \mathbf{H} = 0 \quad \text{and} \quad \text{curl } \mathbf{H} + (i\omega\varepsilon_0 - \underline{\sigma})\mathbf{E} = \mathbf{j} \quad \text{in } \Omega.$$

Here, (\mathbf{E}, \mathbf{H}) represents the electromagnetic field, μ_0 is the magnetic permeability, ε_0 the electric permittivity, ω the angular frequency, \mathbf{j} represents a current density and is supposed to belong to

$$\mathbf{H}_0(\text{div}, \Omega) = \{\mathbf{u} \in \mathbf{L}^2(\Omega) \mid \text{div } \mathbf{u} \in L^2(\Omega), \mathbf{u} \cdot \mathbf{n} = 0 \text{ on } \Gamma\},$$

and $\underline{\sigma}$ is the electric conductivity. We assume that the domain Ω is made of two (connected) subdomains Ω_+ and Ω_- in which the coefficient $\underline{\sigma}$ take two different values ($\sigma_+ = 0, \sigma_- \equiv \sigma$). We denote by Σ the interface between the subdomains Ω_+ and Ω_- . In the most part of our analysis¹, we will assume that the external boundary Γ is contained in the dielectric region $\overline{\Omega}_+$, see Figure 1.

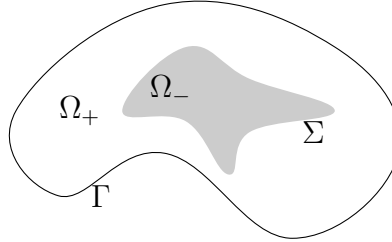


FIGURE 1. The domain Ω and its subdomains Ω_+ (dielectric) and Ω_- (conductor).

To complement the Maxwell harmonic equations (2.1), we consider the perfectly insulating electric boundary conditions on the boundary Γ

$$(2.2) \quad \mathbf{E} \cdot \mathbf{n} = 0 \quad \text{and} \quad \mathbf{H} \times \mathbf{n} = 0 \quad \text{on } \Gamma.$$

Note that we could also consider the perfectly conducting electric boundary conditions $\mathbf{E} \times \mathbf{n} = 0$ and $\mathbf{H} \cdot \mathbf{n} = 0$ on Γ .

¹Except in one configuration in which the roles of the conductor and dielectric bodies are swapped.

2.1. Existence of solutions. Subsequently, we assume that the following condition on the limit problem in the dielectric part Ω_+ is valid:

Assumption 2.1. *The angular frequency ω is not an eigenfrequency of the problem*

$$(2.3) \quad \begin{cases} \operatorname{curl} \mathbf{E} - i\omega\mu_0 \mathbf{H} = 0 & \text{and} & \operatorname{curl} \mathbf{H} + i\omega\varepsilon_0 \mathbf{E} = 0 & \text{in } \Omega_+ \\ \mathbf{E} \times \mathbf{n} = 0 & \text{and} & \mathbf{H} \cdot \mathbf{n} = 0 & \text{on } \Sigma \\ (2.2) & & & \text{on } \Gamma. \end{cases}$$

Hereafter, we denote by $\|\cdot\|_{0,\mathcal{O}}$ the norm in $L^2(\mathcal{O})$. We quote from [3, Th.2.3]:

Theorem 2.2. *If the interface Σ is Lipschitz, under Assumption 2.1, there are constants σ_0 and $C > 0$, such that for all $\sigma \geq \sigma_0$, the Maxwell problem (2.1) with boundary condition (2.2) and data $\mathbf{j} \in \mathbf{H}_0(\operatorname{div}, \Omega)$ has a unique solution (\mathbf{E}, \mathbf{H}) in $L^2(\Omega)^2$, which satisfies:*

$$(2.4) \quad \|\mathbf{E}\|_{0,\Omega} + \|\mathbf{H}\|_{0,\Omega} + \sqrt{\sigma} \|\mathbf{E}\|_{0,\Omega_-} \leq C \|\mathbf{j}\|_{\mathbf{H}(\operatorname{div}, \Omega)}.$$

For convenience, we introduce in the Maxwell equations (2.1) the small parameter

$$(2.5) \quad \delta = \sqrt{\omega\varepsilon_0/\sigma}.$$

Hence, δ tends to 0 when $\sigma \rightarrow \infty$. For $\sigma \geq \sigma_0$, we denote by $(\mathbf{E}_{(\delta)}, \mathbf{H}_{(\delta)})$ the solution of the system (2.1)–(2.2).

2.2. Magnetic formulation. By a standard procedure we deduce from the Maxwell system (2.1)–(2.2) the following variational formulation for the magnetic field $\mathbf{H}_{(\delta)}$. The variational space is $\mathbf{H}_0(\operatorname{curl}, \Omega)$:

$$(2.6) \quad \mathbf{H}_0(\operatorname{curl}, \Omega) = \{\mathbf{u} \in \mathbf{L}^2(\Omega) \mid \operatorname{curl} \mathbf{u} \in \mathbf{L}^2(\Omega), \mathbf{u} \times \mathbf{n} = 0 \text{ on } \Gamma\},$$

and the variational problem writes

Find $\mathbf{H}_{(\delta)} \in \mathbf{H}_0(\operatorname{curl}, \Omega)$ such that for all $\mathbf{K} \in \mathbf{H}_0(\operatorname{curl}, \Omega)$

$$(2.7) \quad \int_{\Omega} \left(\frac{1}{\varepsilon(\delta)} \operatorname{curl} \mathbf{H}_{(\delta)} \cdot \operatorname{curl} \mathbf{K} - \kappa^2 \mathbf{H}_{(\delta)} \cdot \mathbf{K} \right) d\mathbf{x} = \int_{\Omega} \left(\operatorname{curl} \frac{\mathbf{j}}{\varepsilon(\delta)} \right) \cdot \mathbf{K} d\mathbf{x},$$

where we have set

$$(2.8) \quad \varepsilon(\delta) = \mathbf{1}_{\Omega_+} + \left(1 + \frac{i}{\delta^2}\right) \mathbf{1}_{\Omega_-} \quad \text{and} \quad \kappa := \omega \sqrt{\varepsilon_0 \mu_0}.$$

Assumption 2.3. *We assume that the surfaces Σ (interface) and Γ (external boundary) are smooth.*

Under Assumption 2.3, the magnetic field $\mathbf{H}_{(\delta)}$ is globally in $\mathbf{H}^1(\Omega)$.

3. MULTISCALE EXPANSION

Several works are devoted to asymptotic expansions at high conductivity of the electromagnetic field in a domain made of two subdomains *when the interface is smooth*: see [20, 11, 12] for plane interface and eddy current approximation, and [8, 3, 4, 17] for a three-dimensional model of skin effect in electromagnetism.

In this section we recall the results presented in [4] on the behavior of the skin depth function. This relies on asymptotic expansions for the electromagnetic field analyzed in the PhD thesis [17]. For the sake of completeness we give in Appendix A elements of proofs.

Here, we assume that \mathbf{j} is smooth and that Assumptions 2.1 and 2.3 hold. Let \mathcal{U}_- be a tubular neighborhood of the surface Σ in the conductor part Ω_- , see Figure 2. We denote by (y_α, y_3) a local *normal coordinate system* to the surface Σ in \mathcal{U}_- : Here, y_α , $\alpha = 1, 2$, are tangential coordinates on Σ and y_3 is the normal coordinate to Σ , cf. [14, 6].

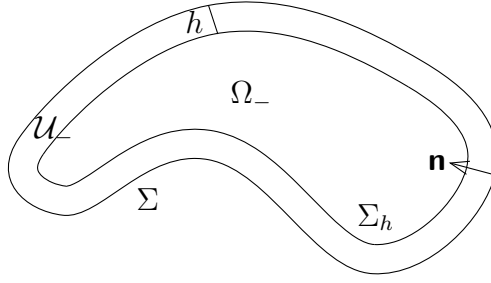


FIGURE 2. A tubular neighbourhood of the surface Σ

In view of our numerical computations, we concentrate on the magnetic field $\mathbf{H}_{(\delta)}$ solution of (2.7). It is denoted by $\mathbf{H}_{(\delta)}^+$ in the dielectric part Ω_+ , and by $\mathbf{H}_{(\delta)}^-$ in the conducting part Ω_- . Both parts exhibit series expansions in powers of δ :

$$(3.1) \quad \mathbf{H}_{(\delta)}^+(\mathbf{x}) = \mathbf{H}_0^+(\mathbf{x}) + \delta \mathbf{H}_1^+(\mathbf{x}) + \mathcal{O}(\delta^2), \quad \mathbf{x} \in \Omega_+$$

$$(3.2) \quad \mathbf{H}_{(\delta)}^-(\mathbf{x}) = \mathbf{H}_0^-(\mathbf{x}; \delta) + \delta \mathbf{H}_1^-(\mathbf{x}; \delta) + \mathcal{O}(\delta^2), \quad \mathbf{x} \in \Omega_-$$

$$(3.3) \quad \text{with } \mathbf{H}_j^-(\mathbf{x}; \delta) = \chi(y_3) \underline{\mathfrak{H}}_j(y_\alpha, \frac{y_3}{\delta}).$$

In (3.1)-(3.2), the symbol $\mathcal{O}(\delta^2)$ means that the remainder is uniformly bounded by δ^2 , and in (3.3), the function $\mathbf{y} \mapsto \chi(y_3)$ is a smooth cut-off with support in $\overline{\mathcal{U}}_-$ and equal to 1 in a smaller tubular neighborhood of Σ . The vector fields $\underline{\mathfrak{H}}_j : (y_\alpha, Y_3) \mapsto \underline{\mathfrak{H}}_j(y_\alpha, Y_3)$ are *profiles* defined on $\Sigma \times \mathbb{R}^+$: They are exponentially decreasing with respect to Y_3 and are smooth in all variables.

3.1. First terms of asymptotics in the conductor region. Hereafter, we present the construction of the first profiles $\underline{\mathfrak{H}}_j = (\mathfrak{H}_j^\alpha, \mathfrak{h}_j)$ and of the first terms \mathbf{H}_j^+ . The normal

component \mathfrak{h}_0 of the first profile in the conductor is zero:

$$\mathfrak{h}_0 = 0.$$

Then, the first term of the magnetic field in the dielectric region solves Maxwell equations with perfectly conducting conditions on Σ :

$$(3.4) \quad \begin{cases} \operatorname{curl} \operatorname{curl} \mathbf{H}_0^+ - \kappa^2 \mathbf{H}_0^+ = \operatorname{curl} \mathbf{j} & \text{in } \Omega_+ \\ \mathbf{H}_0^+ \cdot \mathbf{n} = 0 \quad \text{and} \quad \operatorname{curl} \mathbf{H}_0^+ \times \mathbf{n} = 0 & \text{on } \Sigma \\ \mathbf{H}_0^+ \times \mathbf{n} = 0 \quad \text{and} \quad \operatorname{div} \mathbf{H}_0^+ = 0 & \text{on } \Gamma. \end{cases}$$

Thus the trace \mathbf{h}_0 of \mathbf{H}_0^+ on the interface Σ is *tangential*.

The first profile in the conductor region is exponential with the complex rate λ such that $\lambda^2 = -i\kappa^2$:

$$(3.5) \quad \underline{\mathfrak{H}}_0(y_\beta, Y_3) = \mathbf{h}_0(y_\beta) e^{-\lambda Y_3} \quad \text{with} \quad \lambda = \kappa e^{-i\pi/4}.$$

Note that, if \mathbf{h}_0 is not identically 0, there exists $C_0 > 1$ independent of δ such that

$$(3.6) \quad C_0^{-1} \sqrt{\delta} \leq \|\mathbf{H}_0^-(\cdot; \delta)\|_{0, \Omega_-} \leq C_0 \sqrt{\delta}.$$

The next term which is determined in the asymptotics is the normal component \mathfrak{h}_1 of the profile $\underline{\mathfrak{H}}_1$:

$$(3.7) \quad \mathfrak{h}_1(y_\beta, Y_3) = \lambda^{-1} D_\alpha \mathbf{h}_0^\alpha(y_\beta) e^{-\lambda Y_3}.$$

Here D_α is the covariant derivative on Σ and we use the summation convention of repeated indices. The next term in the dielectric region solves:

$$(3.8) \quad \begin{cases} \operatorname{curl} \operatorname{curl} \mathbf{H}_1^+ - \kappa^2 \mathbf{H}_1^+ = 0 & \text{in } \Omega_+ \\ \mathbf{H}_1^+ \cdot \mathbf{n} = \mathfrak{h}_1 \quad \text{and} \quad \operatorname{curl} \mathbf{H}_1^+ \times \mathbf{n} = i\lambda \mathbf{h}_0 & \text{on } \Sigma \\ \mathbf{H}_1^+ \times \mathbf{n} = 0 \quad \text{and} \quad \operatorname{div} \mathbf{H}_1^+ = 0 & \text{on } \Gamma. \end{cases}$$

Like above, \mathbf{h}_1 is the trace of \mathbf{H}_1^+ on the interface Σ , and \mathbf{h}_1^α denote its tangential components. The tangential components \mathfrak{H}_1^α of the profile $\underline{\mathfrak{H}}_1$ are given by

$$(3.9) \quad \mathfrak{H}_1^\alpha(y_\beta, Y_3) = \left[\mathbf{h}_1^\alpha + Y_3 (H \mathbf{h}_0^\alpha + b_\sigma^\alpha \mathbf{h}_0^\sigma) \right] (y_\beta) e^{-\lambda Y_3}, \quad \alpha = 1, 2.$$

Here $b_\alpha^\gamma = a^{\gamma\beta} b_{\beta\alpha}$, where $a^{\gamma\beta}$ is the inverse of the metric tensor $a_{\alpha\beta}$ in Σ , and $b_{\alpha\beta}$ is the curvature tensor in Σ and

$$H = \frac{1}{2} b_\alpha^\alpha$$

is the *mean curvature* of the surface Σ . In particular, the sign of H depends on the orientation of the surface Σ . As a convention, the unit normal vector \mathbf{n} on the surface Σ is inwardly oriented to Ω_- , see Figure 2.

3.2. Asymptotic behavior of the skin depth. In a one-dimensional model, when the conductor Ω_- is a half-space, the classical *skin depth* parameter is given by

$$(3.10) \quad \ell(\sigma) = \sqrt{\frac{2}{\omega \mu_0 \sigma}}.$$

This length corresponds to the distance from the surface of the conductor where the field has decreased of a rate e . In our situation, following [4, def. 4.1], we extend this definition to curved interfaces. For a data \mathbf{j} , let us define

$$\underline{\mathfrak{H}}_{(\delta)}(y_\alpha, y_3) := \mathbf{H}_{(\delta)}^-(\mathbf{x}), \quad y_\alpha \in \Sigma, \quad 0 \leq y_3 < h_0,$$

for h_0 small enough. Hereafter for any $\mathbf{Z} = (z_1, z_2, z_3) \in \mathbb{C}^3$, $|\mathbf{Z}|$ denotes the vector-norm $(|z_1|^2 + |z_2|^2 + |z_3|^2)^{1/2}$ in \mathbb{C}^3 and $\langle \cdot, \cdot \rangle$ the corresponding hermitian scalar product.

Definition 3.1. Let Σ be a smooth surface, and \mathbf{j} a data of problem (2.1). such that for all y_α in Σ , $\underline{\mathfrak{H}}_{(\delta)}(y_\alpha, 0) \neq 0$. The skin depth is the length $\mathcal{L}(\sigma, y_\alpha)$ defined on Σ and taking the smallest positive value such that

$$(3.11) \quad |\underline{\mathfrak{H}}_{(\delta)}(y_\alpha, \mathcal{L}(\sigma, y_\alpha))| = |\underline{\mathfrak{H}}_{(\delta)}(y_\alpha, 0)| e^{-1}.$$

Thus the length $\mathcal{L}(\sigma, y_\alpha)$ is the distance from the interface where the field has decreased of a fixed rate. It depends on the conductivity σ and of each point y_α in the interface Σ . A priori it also depends on the data \mathbf{j} .

As a consequence of (3.5) and (3.9), there holds

$$(3.12) \quad \begin{cases} |\underline{\mathfrak{H}}_{(\delta)}(y_\alpha, y_3)|^2 = |\mathbf{h}_0(y_\alpha)|^2 \mathfrak{m}(y_\alpha, y_3; \delta) e^{-2y_3 \operatorname{Re}(\lambda)/\delta}, & \text{with} \\ \mathfrak{m}(y_\alpha, y_3; \delta) := \\ 1 + 2y_3 H(y_\alpha) + 2\delta \frac{\operatorname{Re} \langle \mathbf{h}_0(y_\alpha), \mathbf{h}_1(y_\alpha) \rangle}{|\mathbf{h}_0(y_\alpha)|^2} + \mathcal{O}((\delta + y_3)^2). \end{cases}$$

Relying on this formula, one can exhibit the asymptotic behavior of the skin depth $\mathcal{L}(\sigma, y_\alpha)$ for high conductivity σ , cf. [4, Th. 4.2]:

Theorem 3.2. Let Σ be a regular surface with mean curvature H . Recall that $\ell(\sigma)$ is defined by (3.10). We assume that $\mathbf{h}_0(y_\alpha) \neq 0$. The skin depth $\mathcal{L}(\sigma, y_\alpha)$ has the following behavior for high conductivity:

$$(3.13) \quad \mathcal{L}(\sigma, y_\alpha) = \ell(\sigma) \left(1 + H(y_\alpha) \ell(\sigma) + \mathcal{O}(\sigma^{-1}) \right), \quad \sigma \rightarrow \infty.$$

Remark 3.3. The higher order terms $\mathcal{O}(\sigma^{-1})$ in equation (3.13) do depend on the data \mathbf{j} of problem (2.1).

4. AXISYMMETRIC DOMAINS

In order to perform scalar two dimensional computations which could represent correctly the features of a three-dimensional problem, we choose to consider an *axisymmetric configuration* in which Ω_+ and Ω_- are axisymmetric domains with the same axis Ξ_0 :

in *cylindrical coordinates* (r, θ, z) associated with this axis, there exists bi-dimensional “meridian” domains Ω^m and Ω_{\pm}^m such that

$$\begin{aligned}\Omega &= \{\mathbf{x} \in \mathbb{R}^3 \mid (r, z) \in \Omega^m, \theta \in \mathbb{T}\}, \\ \Omega_{\pm} &= \{\mathbf{x} \in \mathbb{R}^3 \mid (r, z) \in \Omega_{\pm}^m, \theta \in \mathbb{T}\}.\end{aligned}$$

Here $\mathbb{T} = \mathbb{R}/(2\pi\mathbb{Z})$ is the one-dimensional torus. We denote by Γ^m and Σ^m the meridian curves corresponding to Γ and Σ , respectively, and by Γ_0, Γ_0^+ the following subsets of the rotation axis Ξ_0 , see Fig. 3

$$\Gamma_0 = \Xi_0 \cap \overline{\Omega}^m \quad \text{and} \quad \Gamma_0^+ = \Xi_0 \cap \overline{\Omega}_+^m.$$

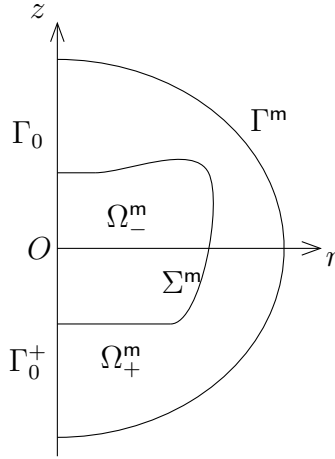


FIGURE 3. The meridian domain $\Omega^m = \Omega_-^m \cup \Omega_+^m \cup \Sigma^m$ with boundary $\partial\Omega^m = \Gamma^m \cup \Gamma_0$

On such an axisymmetric configuration we consider a modification of problem (2.1)-(2.2): We take $\mathbf{j} \equiv 0$ and impose instead of (2.2) non-homogeneous magnetic boundary conditions

$$(4.1) \quad \mathbf{E} \cdot \mathbf{n} = 0 \quad \text{and} \quad \mathbf{H} \times \mathbf{n} = \mathbf{G} \times \mathbf{n} \quad \text{on} \quad \Gamma,$$

for a given data $\mathbf{G} \in \mathbf{H}(\text{curl}, \Omega) := \{\mathbf{u} \in \mathbf{L}^2(\Omega) \mid \text{curl } \mathbf{u} \in \mathbf{L}^2(\Omega)\}$. Then, the variational problem for the magnetic field $\mathbf{H}_{(\delta)}$ solution of the Maxwell equations (2.1)-(4.1) writes

Find $\mathbf{H}_{(\delta)} \in \mathbf{H}_0(\text{curl}, \Omega) + \mathbf{G}$, such that for all $\mathbf{K} \in \mathbf{H}_0(\text{curl}, \Omega)$,

$$(4.2) \quad \int_{\Omega} \left(\frac{1}{\varepsilon(\delta)} \text{curl } \mathbf{H}_{(\delta)} \cdot \text{curl } \mathbf{K} - \kappa^2 \mathbf{H}_{(\delta)} \cdot \mathbf{K} \right) d\mathbf{x} = 0.$$

4.1. Formulation in cylindrical components. For a vector field $\mathbf{H} = (H_1, H_2, H_3)$, we introduce its *cylindrical components* (H_r, H_θ, H_z) according to

$$\begin{cases} H_r(r, \theta, z) &= H_1(\mathbf{x}) \cos \theta + H_2(\mathbf{x}) \sin \theta, \\ H_\theta(r, \theta, z) &= -H_1(\mathbf{x}) \sin \theta + H_2(\mathbf{x}) \cos \theta, \\ H_z(r, \theta, z) &= H_3(\mathbf{x}), \end{cases}$$

and we set

$$\check{\mathbf{H}}(r, \theta, z) = (H_r(r, \theta, z), H_\theta(r, \theta, z), H_z(r, \theta, z)).$$

We say that \mathbf{H} is axisymmetric if $\check{\mathbf{H}}$ does not depend on the angular variable θ .

The Maxwell problem (4.2) is axisymmetric, which means that, expressed in cylindrical variables (r, θ, z) and components $\check{\mathbf{H}}$, its coefficients do not depend on θ [9, 1, 15]. Recall that for a vector field $\mathbf{H} = (H_1, H_2, H_3)$ the *cylindrical components* of its curl write

$$(4.3) \quad \begin{cases} (\text{curl } \mathbf{H})_r = \frac{1}{r} \partial_\theta H_z - \partial_z H_\theta, \\ (\text{curl } \mathbf{H})_\theta = \partial_z H_r - \partial_r H_z, \\ (\text{curl } \mathbf{H})_z = \frac{1}{r} (\partial_r (r H_\theta) - \partial_\theta H_r). \end{cases}$$

As a consequence, if the right-hand side \mathbf{G} is axisymmetric, and if (4.2) has a unique solution, then this solution is axisymmetric. According to (4.3), when \mathbf{H} is axisymmetric its curl reduces to

$$(4.4) \quad \begin{cases} (\text{curl } \mathbf{H})_r = -\partial_z H_\theta, \\ (\text{curl } \mathbf{H})_\theta = \partial_z H_r - \partial_r H_z, \\ (\text{curl } \mathbf{H})_z = \frac{1}{r} \partial_r (r H_\theta). \end{cases}$$

4.2. Axisymmetric orthoradial problem. We say that \mathbf{H} is orthoradial if its components H_r and H_z are zero.

We assume that \mathbf{G} is axisymmetric and orthoradial, i.e.,

$$\check{\mathbf{G}}(r, \theta, z) = (0, g(r, z), 0).$$

The components (H_r, H_z) and H_θ being uncoupled in (4.4), and the solution of problem (4.2) being unique, we obtain that this solution is orthoradial

$$\check{\mathbf{H}}_{(\delta)}(r, \theta, z) = (0, h_{(\delta)}(r, z), 0).$$

4.2.1. Variational formulation. In this framework, the change from Cartesian to cylindrical coordinates requires the modification of the solution spaces $\mathbf{H}_0(\text{curl}, \Omega)$ used in problem (4.2). Precisely, the weighted space characterizing the *orthoradial component* $h_{(\delta)}(r, z)$ is

$$V_{1, \Gamma^m}^1(\Omega^m) = \{v \in H_1^1(\Omega^m) \mid v \in L_{-1}^2(\Omega^m) \text{ and } v = 0 \text{ on } \Gamma^m\}.$$

Here,

$$H_1^1(\Omega^m) = \{v \in L_1^2(\Omega^m) \mid \partial_r^j \partial_z^{1-j} v \in L_1^2(\Omega^m), j = 0, 1\},$$

and for all $\alpha \in \mathbb{R}$, the space $L_\alpha^2(\Omega^m)$ is the set of measurable functions $v(r, z)$ such that

$$\|v\|_{L_\alpha^2(\Omega^m)}^2 = \int_{\Omega^m} |v|^2 r^\alpha dr dz < +\infty .$$

Remark 4.1. The space $V_{1,\Gamma^m}^1(\Omega^m)$ incorporates essential boundary conditions, in particular on Γ_0 , where $v = 0$, see [1, Remark II.1.1].

This leads us to solve the following two-dimensional scalar problem set in Ω^m .

Find $h_{(\delta)} \in V_{1,\Gamma^m}^1(\Omega^m) + g$ such that for all $w \in V_{1,\Gamma^m}^1(\Omega^m)$,

$$(4.5) \quad a^\delta(h_{(\delta)}, w) = 0 ,$$

where

$$a^\delta(h, w) := \int_{\Omega^m} \frac{1}{\varepsilon(\delta)} \left(\partial_z h \partial_z w + \frac{1}{r} \partial_r(rh) \frac{1}{r} \partial_r(rw) \right) r dr dz - \kappa^2 \int_{\Omega^m} h w r dr dz .$$

4.2.2. Asymptotic expansion. Let $(r(\xi), z(\xi)) = \boldsymbol{\tau}(\xi)$, $\xi \in (0, L)$, be an *arc-length coordinate* on the interface Σ^m . Here $\xi \mapsto \boldsymbol{\tau}(\xi)$ is a C^∞ function, and L is the length of the curve Σ^m . Let (ξ, y_3) be the associate normal coordinate system in a tubular neighborhood of Σ^m inside Ω_-^m . Then the normal vector $\mathbf{n}(\xi)$ at the point $\boldsymbol{\tau}(\xi)$ can be written as (Frenet frame)

$$(4.6) \quad \mathbf{n}(\xi) = (-z'(\xi), r'(\xi)) \quad \text{with} \quad z'(\xi) = \frac{dz}{d\xi} \quad \text{and} \quad r'(\xi) = \frac{dr}{d\xi} .$$

Finally we denote by $k(\xi)$ the curvature of Σ^m in $\boldsymbol{\tau}(\xi)$.

In accordance with (3.1)-(3.2)-(3.3), we can exhibit series expansions in powers of δ for the magnetic field $h_{(\delta)}$ which we denote by $h_{(\delta)}^+$ in the dielectric part Ω_+ , and by $h_{(\delta)}^-$ in the conducting part Ω_- :

$$h_{(\delta)}^+(r, z) = h_0^+(r, z) + \delta h_1^+(r, z) + \mathcal{O}(\delta^2) ,$$

$$h_{(\delta)}^-(r, z) = h_0^-(r, z; \delta) + \delta h_1^-(r, z; \delta) + \mathcal{O}(\delta^2), \quad h_j^-(r, z; \delta) = \chi(y_3) h_j^\theta(\xi, \frac{y_3}{\delta}) .$$

Here the profiles h_j^θ are defined on $\Sigma^m \times \mathbb{R}^+$. Hereafter, we focus on the first terms h_0^+ , h_0^θ , h_1^+ , and h_1^θ . We introduce the interior and boundary operators

$$(4.7) \quad D(r, z; \partial_r, \partial_z) = \partial_r^2 + \frac{1}{r} \partial_r + \partial_z^2 - \frac{1}{r^2}$$

$$\text{and} \quad B(\xi; \partial_r, \partial_z) = -z'(\xi) \left(\partial_r + \frac{1}{r} \right) + r'(\xi) \partial_z .$$

In appendix B.1, we give the expansion of these operators in power series of δ inside the domain Ω_- and on the interface Σ^m . The terms h_0^+ , h_0^θ , h_1^+ , and h_1^θ satisfy the following problems coupled by their boundary conditions on the interface Σ^m (corresponding to

$Y = 0$) – compare with (3.4)-(3.5), (3.8)-(3.9):

$$(4.8) \quad \begin{cases} Dh_0^+ + \kappa^2 h_0^+ &= 0 & \text{in } \Omega_+^m, \\ Bh_0^+ &= 0 & \text{on } \Sigma^m, \\ h_0^+ &= g & \text{on } \Gamma^m \cup \Gamma_0^+, \end{cases}$$

$$(4.9) \quad \begin{cases} (\partial_Y^2 - \lambda^2) h_0^\theta &= 0 & \text{for } 0 < Y < +\infty, \\ h_0^\theta &= h_0^+ & \text{for } Y = 0, \end{cases}$$

with λ defined by (3.5), from which we deduce:

$$(4.10) \quad h_0^\theta(\xi, Y) = e^{-\lambda Y} h_0^+(\tau(\xi)).$$

The next problem in the dielectric part is

$$(4.11) \quad \begin{cases} Dh_1^+ + \kappa^2 h_1^+ &= 0 & \text{in } \Omega_+^m, \\ Bh_1^+ &= -i\partial_Y h_0^\theta & \text{on } \Sigma^m, \\ h_1^+ &= 0 & \text{on } \Gamma^m \cup \Gamma_0^+, \end{cases}$$

Thus (4.10) yields that h_1^+ satisfies $Bh_1^+ = i\lambda h_0^+|_{\Sigma^m}$ on the interface.

The next problem in the conductor part is

$$(4.12) \quad \begin{cases} (\partial_Y^2 - \lambda^2) h_1^\theta &= -A_1 h_0^\theta & \text{for } 0 < Y < +\infty, \\ h_1^\theta &= h_1^+ & \text{for } Y = 0. \end{cases}$$

Here, $A_1 h_0^\theta = -(k + \frac{z'}{r})(\xi) \partial_Y h_0^\theta$. From (4.10), we infer $A_1 h_0^\theta = e^{-\lambda Y} \lambda (k + \frac{z'}{r})(\xi) h_0^+|_{\Sigma^m}$. Then, from equation (4.12), we obtain

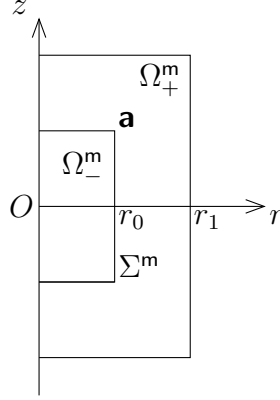
$$(4.13) \quad h_1^\theta(\xi, Y) = e^{-\lambda Y} \left[h_1^+(\tau(\xi)) + \frac{Y}{2} \left(k + \frac{z'}{r} \right)(\xi) h_0^+(\tau(\xi)) \right].$$

Note that we can also deduce this profile h_1^θ from equations (3.5) and (3.9), but this is not obvious because the cylindrical coordinates are not a normal coordinate system, see Appendix B.2.

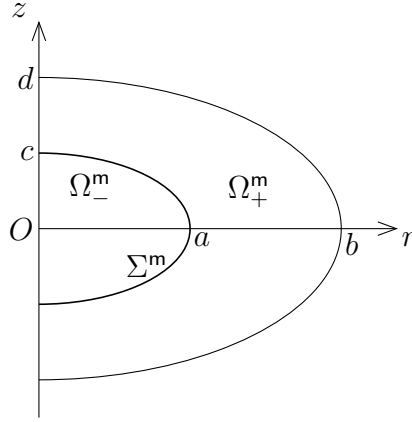
Remark 4.2. Subsequently, we assume that the data g is a real valued function. Thus, the right hand side of the boundary value problem (4.8) is real. Hence h_0^+ is a real valued function. Recall that $Bh_1^+ = \kappa e^{i\pi/4} h_0^+|_{\Sigma}$. From the boundary value problem (4.11), we infer: $\text{Re } h_1^+ = \text{Im } h_1^+$. We will exploit this relationship in the numerical simulations of skin effect, see §6.

4.3. Configurations chosen for computations. We consider three classes of geometric configurations: one cylindrical configuration (A) and two spheroidal configurations (B and C).

Configuration A: cylindrical geometry. We assume that Ω is a circular cylinder of radius r_1 and length ℓ_1 , and Ω_- is a coaxial cylinder of radius r_0 and length ℓ_0 . Hence, Ω^m is a rectangle of width r_1 and length ℓ_1 , and Ω_-^m is a coaxial rectangle of width r_0 and length ℓ_0 , see Figure 4. We choose the parameters $r_0 = 1$, $\ell_0 = 2$, $r_1 = 2$, $\ell_1 = 4$ in computations.

FIGURE 4. The meridian domain Ω^m in configuration A

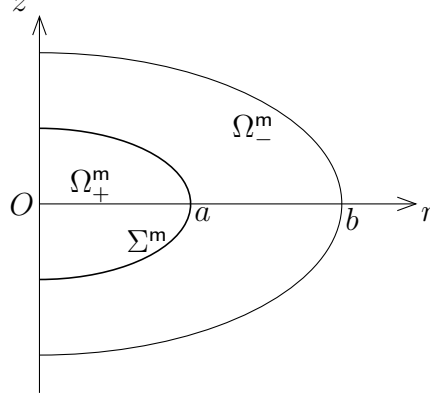
Configuration B: spheroidal geometry. We assume that Ω is a spheroid, and Ω_- is a coaxial spheroid. We denote by a and c , respectively b and d , the semimajor and semiminor axis of Ω_- , respectively Ω . Hence, Ω^m is a semi-ellipse with semimajor axis b and semiminor axis d , and Ω_-^m is a coaxial semi-ellipse with axis lengths a and c , see Figure 5. In computations, we consider the following parameters

FIGURE 5. The meridian domain Ω^m in configuration B1

$$(4.14) \quad \begin{aligned} \text{Configuration B1: } & a = 2, b = 4, c = 1, d = 2, \text{ (oblate spheroid)} \\ \text{Configuration B2: } & a = 4, b = 8, c = 1, d = 2, \text{ (more oblate spheroid).} \end{aligned}$$

Note that all the numerical parameters are given in SI units, in particular, a, b, c , and d are defined in meters, and the conductivity σ is defined in siemens per meter $S.m^{-1}$.

Configuration C: spheroidal geometry. We introduce a configuration C, switching the roles of the subdomains Ω_-^m and Ω_+^m in the configuration B, see Figure 6. We denote by

FIGURE 6. The meridian domain Ω^m in configuration C1

C1 and C2 the configuration C, which correspond to the choice of parameters a, b, c, d , see (4.14).

Right hand sides of problems. In configurations A and B, we take the data $g = r$. Hence, $h_{(\delta)}$ satisfies the following inhomogeneous Dirichlet boundary condition

$$h_{(\delta)}(r, z) = r \quad \text{on} \quad \Gamma^m.$$

For configuration C1, we take $g = 0$ and an interior data $f := (\text{curl} \mathbf{j})_\theta$ with support inside Ω_+^m : $f = 10^2$ if $r^2/4 + z^2 \leq 0.8$ and $f = 0$ otherwise.

5. FINITE ELEMENT DISCRETIZATIONS AND COMPUTATIONS

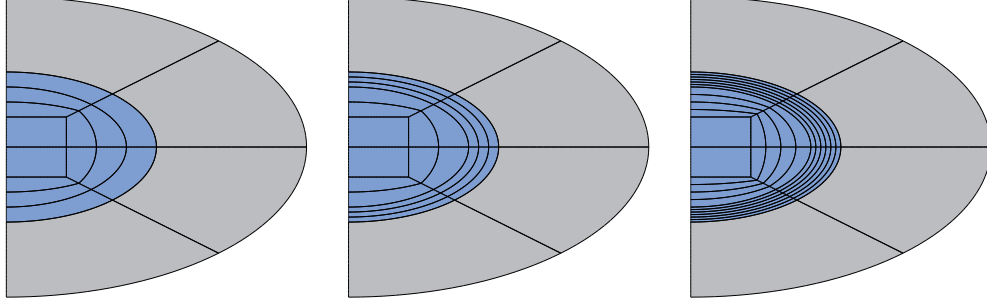
5.1. Finite element method. In this section, we consider two benchmarks for the computational domain: configuration A, see Figure 4, and configuration B, see Figure 5. We use high order elements available in the finite element library Mélima, see [13], and quadrangular meshes in the meridian domain. We discretize the variational problem (4.5). The script used to solve the problem (4.5) is adapted from [2]. In the computations, we fix the angular frequency $\omega = 3 \cdot 10^7$. We denote by $h_{(\delta)}^{p, \mathfrak{M}}$ the computed solution of the discretized problem (4.5) with an interpolation degree p and a mesh \mathfrak{M} . We define

$$A_\sigma^{p, \mathfrak{M}} := \|h_{(\delta)}^{p, \mathfrak{M}}\|_{L_1^2(\Omega_-^m)} \quad \text{with} \quad \sigma = \omega \varepsilon_0 \delta^{-2}, \quad \text{cf. (2.5)}.$$

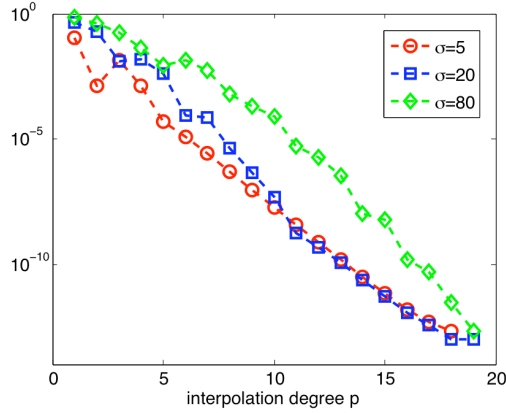
5.2. Interpolation degree. We first check the convergence when the interpolation degree of the finite elements increases.

5.2.1. Configuration B1. We consider the discretized problem with different degrees: Q_p^2 , for all $p = 1, \dots, 20$, and with three different meshes $\mathfrak{M}_1, \mathfrak{M}_3$ and \mathfrak{M}_6 with 1, 3 or 6 layers of elongated elements in the skin region of the conductor Ω_-^m , see Figure 7.

²Recall that Q_p is the vector space of polynomials of two variables and partial degree p defined on the reference element $\widehat{K} := [0, 1] \times [0, 1]$

FIGURE 7. The meshes \mathfrak{M}_1 , \mathfrak{M}_3 and \mathfrak{M}_6 for configuration B1

We represent in Figure 8 the absolute value of the difference between the weighted norms $A_\sigma^{p, \mathfrak{M}_1}$ and $A_\sigma^{20, \mathfrak{M}_6}$, versus p in semilogarithmic coordinates, and in each case: $\sigma = 5$ with circles, $\sigma = 20$ with squares, and $\sigma = 80$ with diamonds. We refer to [19] for theoretical results of convergence for the p -version in presence of an exponentially decreasing boundary layer. In Figure 9 we use mesh \mathfrak{M}_3 instead of \mathfrak{M}_1 .

FIGURE 8. Graph of $|A_\sigma^{p, \mathfrak{M}_1} - A_\sigma^{20, \mathfrak{M}_6}|$ with respect to $p = 1, \dots, 19$ in semi-log coordinates, for $\sigma \in \{5, 20, 80\}$ and configuration B1

In Figure 10, we plot in log-log coordinates the weighted norm $A_\sigma^{16, \mathfrak{M}_3}$ with respect to $\sigma = 5, 20, 80, 100, 200, 300, 400$ with circles, and the graph of $\sigma \mapsto \sigma^{-1/4}$ by a solid line. The figure shows that $A_\sigma^{16, \mathfrak{M}_3}$ behaves like $\sigma^{-1/4}$ when $\sigma \rightarrow \infty$. This behavior is consistent with the asymptotic expansion (3.2) and the estimate (3.6), (recall formula (2.5)).

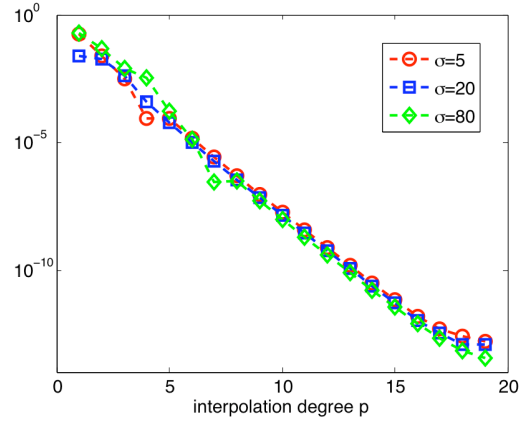


FIGURE 9. Graph of $|A_{\sigma}^{p, \mathfrak{M}_3} - A_{\sigma}^{20, \mathfrak{M}_6}|$ with respect to $p = 1, \dots, 19$ in semi-log coordinates, for $\sigma \in \{5, 20, 80\}$ and configuration B1

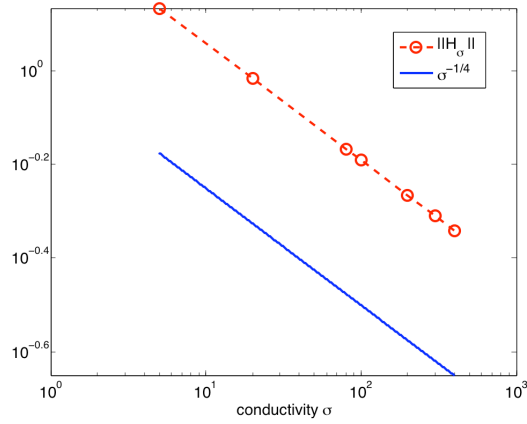


FIGURE 10. In circle: $A_{\sigma}^{16, \mathfrak{M}_3}$ for $\sigma = 5, 20, 80, 100, 200, 300, 400$. In solid line: the graph of the function $\sigma \mapsto \sigma^{-1/4}$ in log-log coordinates for configuration B1

5.2.2. *Configuration A.* We consider a family of eight meshes with square elements \mathfrak{M}_k , $k = 1, \dots, 8$ with size $h = 1/k$, see Figure 11. We represent in Figure 12 the

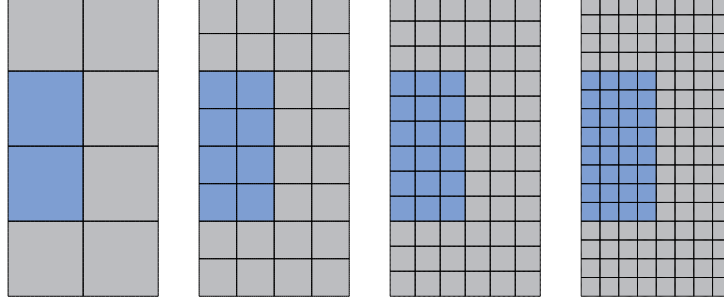


FIGURE 11. Meshes \mathfrak{M}_1 , \mathfrak{M}_2 , \mathfrak{M}_3 , and \mathfrak{M}_4 for configuration A

absolute value of the difference between $A_\sigma^{p, \mathfrak{M}_2}$ and $A_\sigma^{16, \mathfrak{M}_3}$, versus p in semilogarithmic coordinates, and in each case: $\sigma = 5$ with circles, $\sigma = 20$ with squares, and $\sigma = 80$ with diamonds. The figure shows that $A_\sigma^{p, \mathfrak{M}_2}$ approximates $A_\sigma^{16, \mathfrak{M}_3}$ better than 10^{-4} when $p \geq 12$.

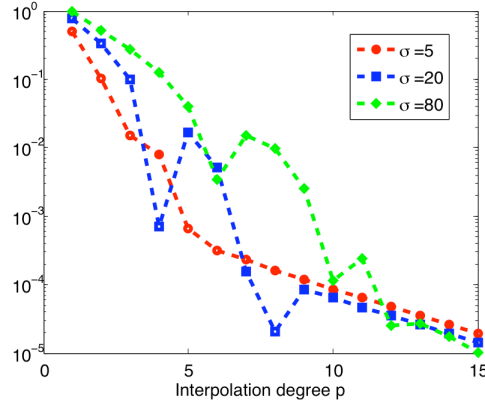


FIGURE 12. Graph of $|A_\sigma^{p, \mathfrak{M}_2} - A_\sigma^{16, \mathfrak{M}_3}|$ with respect to $p = 1, \dots, 15$ in semi-log coordinates, for $\sigma \in \{5, 20, 80\}$ for configuration A

5.3. Stability of the h-version. In this subsection, we check the convergence of the discretized problem in configuration A for several meshes \mathfrak{M}_k of the computational domain when k increases. We fix the interpolation degree $p = 2$ of the finite elements and use the square meshes \mathfrak{M}_k . We plot in Figure 13 the absolute value of the difference between $A_\sigma^{2,\mathfrak{M}_k}$ and $A_\sigma^{6,\mathfrak{M}_8}$ with respect to $k = 1, \dots, 8$, in log-log coordinates.

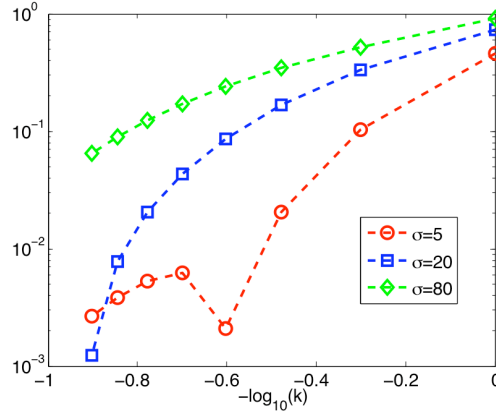


FIGURE 13. Graph of $|A_\sigma^{2,\mathfrak{M}_k} - A_\sigma^{6,\mathfrak{M}_8}|$ with respect to $-\log_{10}(k)$ in semi-log coordinates, when $k = 1, \dots, 8$ and $\sigma = 5, 20, 80$ for configuration A

6. NUMERICAL SIMULATIONS OF SKIN EFFECT

Recall that the asymptotic expansion of $h_{(\delta)}$ is described in §4.2.2. According to Remark 4.2 the first term h_0^+ is a real valued function. Hence the imaginary part of the magnetic field $h_{(\delta)}$ is small in the dielectric Ω_+^m , because

$$|\operatorname{Im} h_{(\delta)}^+| = \mathcal{O}(\delta).$$

Thus, the imaginary part of the computed field is located in the conductor Ω_-^m . We display this imaginary part to highlight the boundary layer near the surface of the conductor, see Figures 15, 16 bottom, 17 and 18. In this section, $\tilde{h}_\sigma := h_{(\delta)}^{p,\mathfrak{M}_k}$ denote the computed solution associated with the numerical parameters considered in each subsection.

6.1. Skin effect in configuration A. We fix the mesh \mathfrak{M}_2 , see Figure 11, and the interpolation degree of the finite elements : $p = 16$. Here $\tilde{h}_\sigma = h_{(\delta)}^{16,\mathfrak{M}_2}$ is computed in configuration A for several values of σ , see Figure 14. Similarly, we compute $|\operatorname{Im} \tilde{h}_\sigma|$, see Figure 15.

6.2. Skin effect in configuration B. Here $\tilde{h}_\sigma = h_{(\delta)}^{p,\mathfrak{M}_3}$ is the computed solution for several values of σ , with a fixed mesh \mathfrak{M}_3 (Figure 7). We represent $|\tilde{h}_\sigma|$ and $|\operatorname{Im} \tilde{h}_\sigma|$ in configuration B1, with an interpolation degree $p = 16$, see Figure

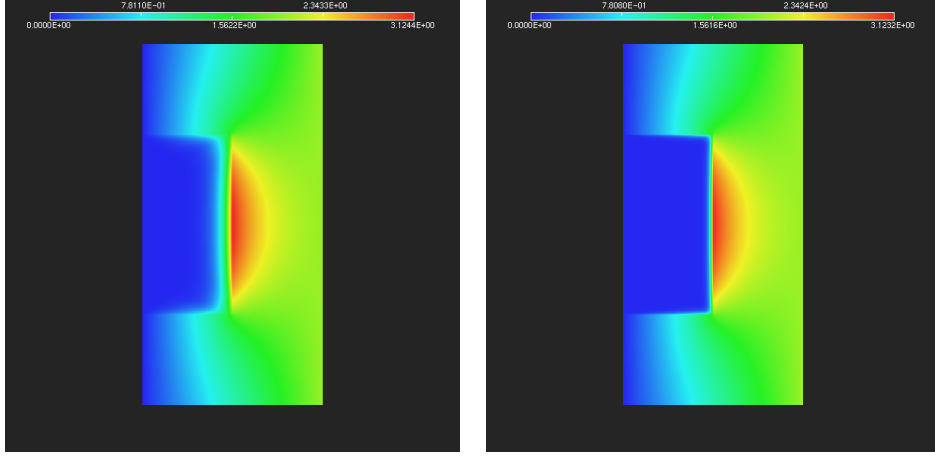


FIGURE 14. Configuration A. On the left, $|\tilde{h}_\sigma|$ when $\sigma = 5$. On the right, $|\tilde{h}_\sigma|$ when $\sigma = 80$

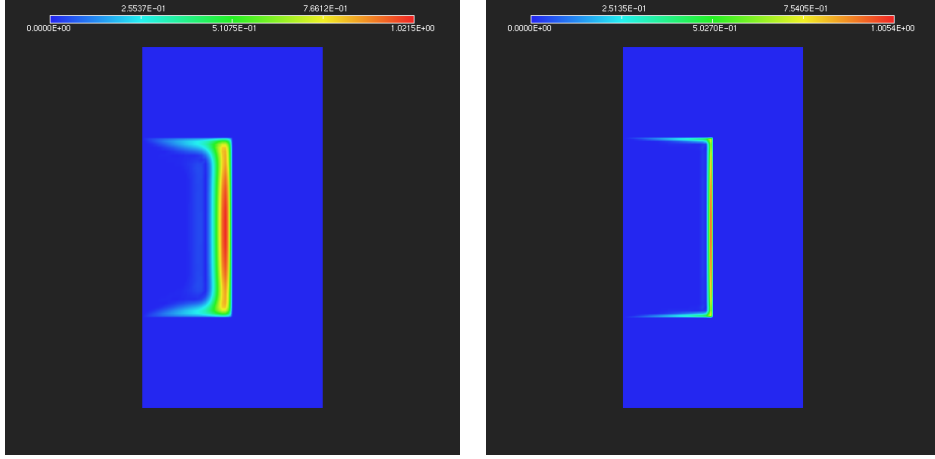


FIGURE 15. Configuration A. On the left, $|\text{Im } \tilde{h}_\sigma|$ when $\sigma = 5$. On the right, $|\text{Im } \tilde{h}_\sigma|$ when $\sigma = 80$

6.3. Skin effect in configurations B and C. In order to exhibit the influence of the sign of the mean curvature H of the interface Σ on the skin effect, we fix in this subsection the conductivity $\sigma = 5$. We perform computations in configurations B and C. We note that $H > 0$ in configuration B, and $H < 0$ in configuration C. We compute $|\text{Im } \tilde{h}_\sigma|$ in configurations B1 and C1, see Figure 17. We then compute $|\text{Im } \tilde{h}_\sigma|$ in configurations B2 and C2: $H > 0$, and $H < 0$, see Figure 18.

Figures 17 and 18 show that the skin depth is larger for a fixed conductivity when the mean curvature of the conducting body surface is larger. Moreover, the sign of the

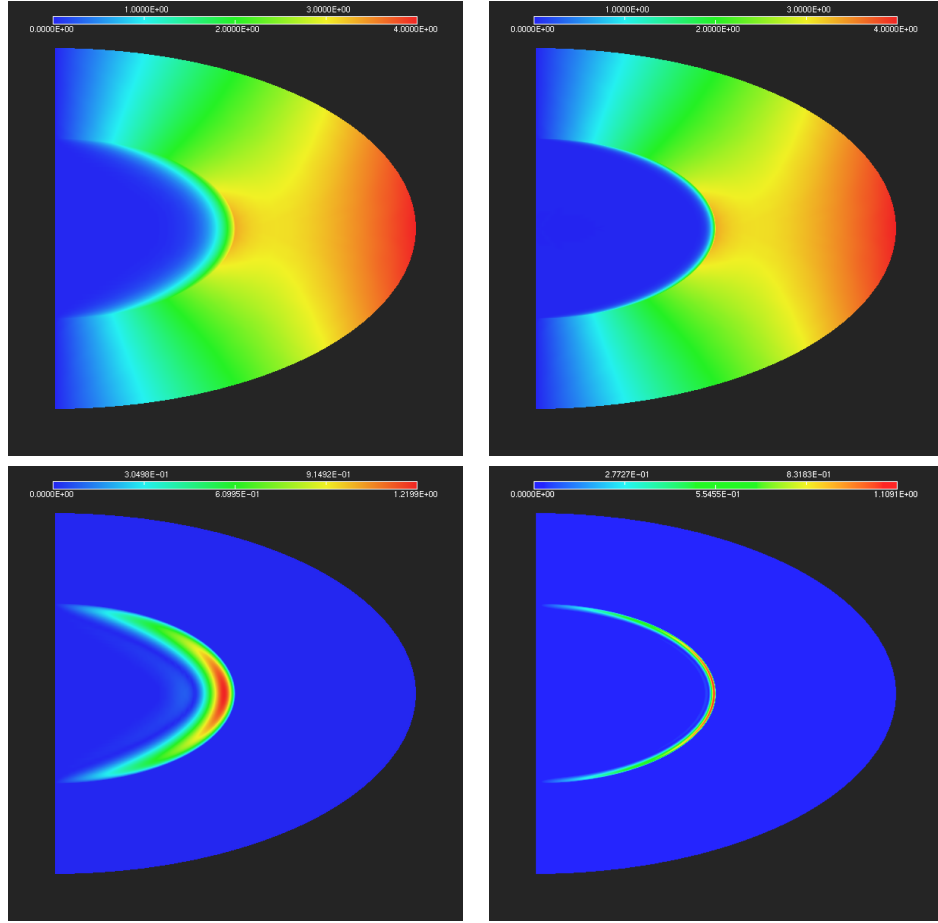


FIGURE 16. Configuration B1. At the top, $|\tilde{h}_\sigma|$ when $\sigma = 5$ (on the left), and $\sigma = 80$ (on the right). At the bottom, $|\operatorname{Im} \tilde{h}_\sigma|$ when $\sigma = 5$ and $\sigma = 80$

curvature has an influence on the skin depth. This length is larger in convex (Figures 17 and 18 on the left) than in concave conductors (same figures on the right).

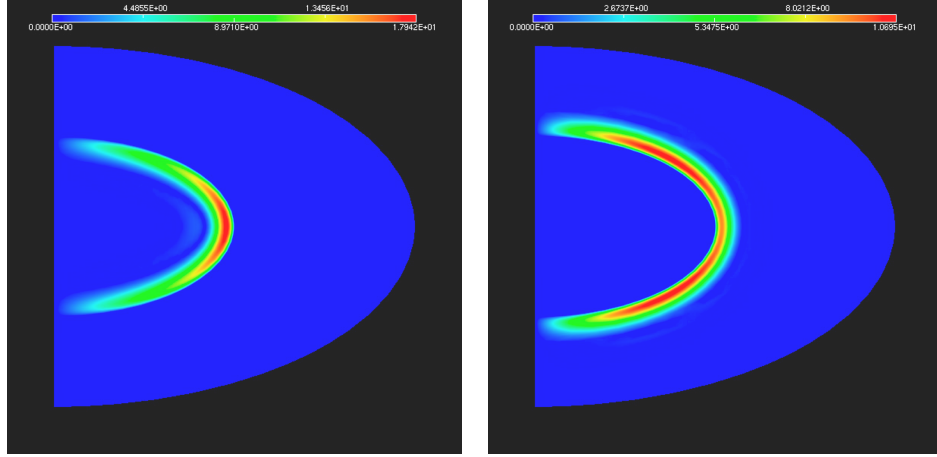


FIGURE 17. On the left, $|\operatorname{Im} \tilde{h}_\sigma|$ in configuration B1 ($H > 0$). On the right, $|\operatorname{Im} \tilde{h}_\sigma|$ in configuration C1 ($H < 0$). $\sigma = 5$

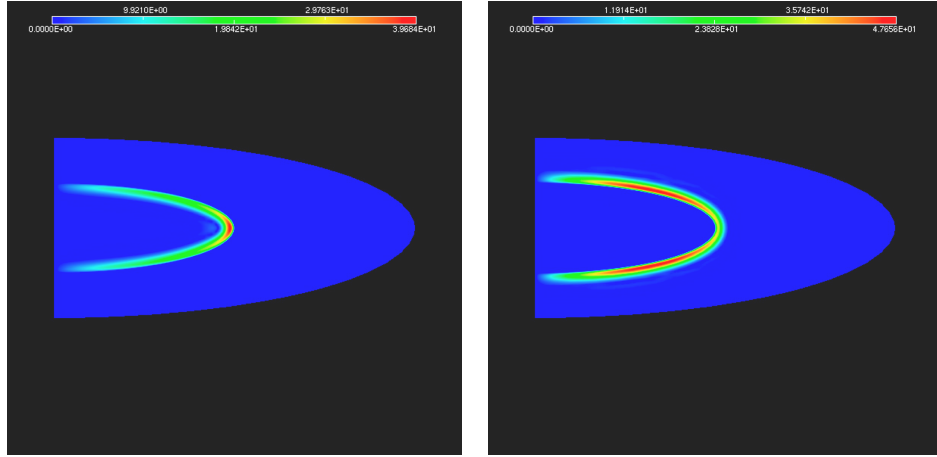


FIGURE 18. On the left, $|\operatorname{Im} \tilde{h}_\sigma|$ in configuration B2. On the right, $|\operatorname{Im} \tilde{h}_\sigma|$ in configuration C2. $\sigma = 5$

7. POSTPROCESSING

In this section, we perform numerical treatments from computations in configuration B1, see subsection 6.2, and configuration A, see subsection 6.1, in order to investigate whether solutions are exponentially decreasing inside the conductor and with which rate. Let us recall that the standard skin depth $\ell(\sigma)$ is given by (3.10).

7.1. Configuration B. The mesh of the computational domain is the mesh \mathfrak{M}_3 , see Figure 7. We extract values of $|\tilde{h}_\sigma|$ in Ω_-^m along edges of the mesh \mathfrak{M}_3 for $z = 0$: in this configuration, the normal coordinate writes $y_3 := 2 - r$.

Then, we perform a linear regression from values of $\log_{10} |\tilde{h}_\sigma(y_3)|$ in the skin depth $\ell(\sigma)$, see Figure 19. We denote by $n(\sigma)$ the number of extracted values on the axis $z = 0$ in the skin depth $\ell(\sigma)$. From the linear regression, we derive a numerical slope $\tilde{s}(\sigma)$ such that

$$\log_{10} |\tilde{h}_\sigma(y_3)| = -\tilde{s}(\sigma)y_3 + b, \quad b \in \mathbb{R}.$$

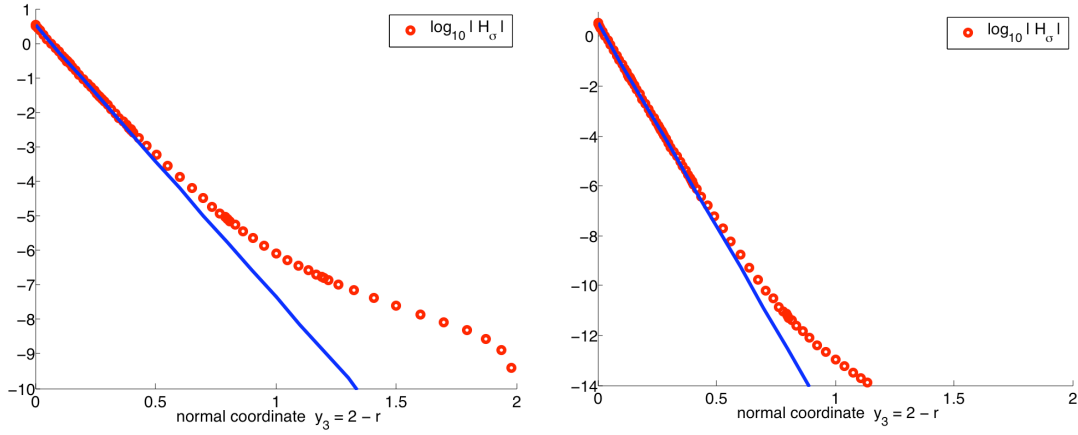


FIGURE 19. In circles, extracted values of $\log_{10} |\tilde{h}_\sigma(y_3)|$. In solid line, linear regression of $\log_{10} |\tilde{h}_\sigma(y_3)|$. On the left $\sigma = 20$ (interpolation degree $p = 12$). On the right, $\sigma = 80$ (degree $p = 16$). $n(20) = 6$, $\tilde{s}(20) = 7.86906$ and $n(80) = 5$, $\tilde{s}(80) = 16.29634$. Configuration B1

Accuracy of asymptotics. Relying on formula (3.12), we can derive a Taylor expansion of $\log_{10} |\mathfrak{H}_{(\delta)}(y_\alpha, y_3)|$ with respect to y_3 : for y_3 small enough

$$(7.1) \quad \log_{10} |\mathfrak{H}_{(\delta)}(y_\alpha, y_3)| = \log_{10} |\mathbf{h}_0(y_\alpha)| - s(y_\alpha, \sigma)y_3 + \frac{\delta}{\ln 10} |\mathbf{h}_0(y_\alpha)|^{-2} \operatorname{Re} \langle \mathbf{h}_0(y_\alpha), \mathbf{h}_1(y_\alpha) \rangle + \mathcal{O}((\delta + y_3)^2).$$

Here the function

$$s(y_\alpha, \sigma) := \frac{1}{\ln 10} \left(\frac{1}{\ell(\sigma)} - H(y_\alpha) \right)$$

depends on the skin depth $\ell(\sigma)$ and the mean curvature $H(y_\alpha)$ at the point y_α of the interface Σ . We note that the mean curvature of the surface Σ is constant when $z = 0$. Hence, we introduce hereafter the theoretical slope

$$s(\sigma) := s(y_\alpha, \sigma) \quad \text{when } z = 0.$$

In configuration B1, the principal curvatures at a point of the interface Σ when $z = 0$ are the constants $\kappa_1 = 2$ and $\kappa_2 = \frac{1}{2}$. Hence, $H(y_\alpha) = \frac{5}{4}$. We infer

$$s(\sigma) = \frac{1}{\ln 10} \left(\frac{1}{\ell(\sigma)} - \frac{5}{4} \right).$$

The accuracy of the asymptotic expansion is tested by representing the relative error between numerical and theoretical slopes:

$$\text{err}(\sigma) := \left| \frac{s(\sigma) - \tilde{s}(\sigma)}{s(\sigma)} \right|,$$

see the table 1. In order to make clear whether the influence of the curvature is visible in computations, we also display the theoretical curvature ratio

$$\text{curv_ratio}(\sigma) := \frac{\frac{5}{4}}{\frac{1}{\ell(\sigma)} - \frac{5}{4}}.$$

σ	5	20	80
$\ell(\sigma)$	0.103	0.0515	0.0258
$s(\sigma)$	3.67332	7.88951	16.32188
$\text{curv_ratio}(\sigma)$	0.148	0.069	0.033
degree p	10	12	16
$n(\sigma)$	7	6	5
$\tilde{s}(\sigma)$	3.64686	7.87347	16.308279
$\text{err}(\sigma)$	0.0072	0.002	0.0008

TABLE 1. Postprocessing in configuration B1 with the mesh \mathfrak{M}_3

The relative error decreases more than a half when the conductivity is multiplied by 4. Anyway, this relative error is much smaller than $\text{curv_ratio}(\sigma)$, which exhibits numerically the influence of the curvature on the skin depth. We perform similar computations with the mesh \mathfrak{M}_6 represented in Figure 7, see Table 2, and obtain still better results.

Remark 7.1. A similar postprocessing along the r -axis was performed for configuration A, see [17, Ch. 8, §8.3.2]. Relative errors $\text{err}(\sigma)$ are still consistent with the expansion (7.1). Non-radial postprocessings was performed along the segment OL , when L is the point with a colatitude φ_0 in the interface Σ^m , see Figure 20: when $\varphi_0 = \pi/2 - \arctan(1/2)$ (i.e. $r_L = \sqrt{2}, z_L = 1/\sqrt{2}$), see [17, Ch. 8, §8.5.1]. Relative errors are again very small.

σ	5	20	80
degree p	8	12	16
$n(\sigma)$	13	9	7
$\tilde{s}(\sigma)$	3.64239	7.88170	16.33051
$\text{err}(\sigma)$	0.0084	0.001	0.0005

TABLE 2. Postprocessing in configuration B1 with the mesh \mathfrak{M}_6 (see Table 1 for the theoretical values $\ell(\sigma)$, $s(\sigma)$, and $\text{curv_ratio}(\sigma)$)

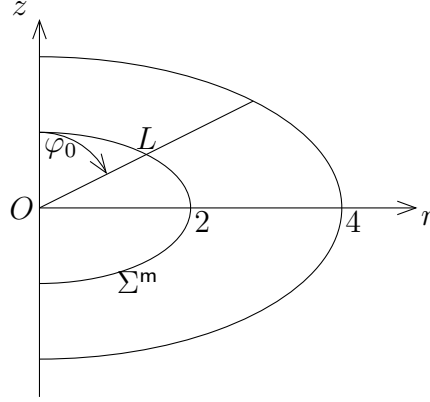


FIGURE 20. In the meridian domain in configuration B1, L is the point on Σ^m with a colatitude $\varphi_0 = \pi/2 - \arctan(1/2)$

7.2. Configuration A. The mesh of the computational domain is the mesh \mathfrak{M}_4 represented in Figure 11. We extract values of $\log_{10} |\tilde{h}_\sigma|$ in Ω_-^m along the diagonal axis $r = z$, see Figure 21: here we denote by

$$\rho := \sqrt{(1-r)^2 + (1-z)^2},$$

the distance to the corner point **a** with coordinates $(r = 1, z = 1)$, cf. Figure 4.

When compared with Figure 19, we see that the curves do not exactly behave like lines, which means that the exponential decay is not obvious. In order to measure a possible exponential decay, we define the slopes $\tilde{s}_i(\sigma)$ of extracted values $\log_{10} |\tilde{h}_\sigma(\rho)|$ by:

$$\tilde{s}_i(\sigma) := \frac{\log_{10} |\tilde{h}_\sigma(r_i, z_i)| - \log_{10} |\tilde{h}_\sigma(z_{i+1}, r_{i+1})|}{\rho_{i+1} - \rho_i}.$$

Here, ρ_i is the distance to the corner point **a** defined by $\rho_i := \sqrt{(1-r_i)^2 + (1-z_i)^2}$ with (r_i, z_i) the extraction points. We present in the Figure 22 the graph of the slopes $\tilde{s}_i(\sigma)$ for each curve on the Figure 21 ($\sigma = 20, 80$). For the sake of comparison, we also represent on the same figure the slopes of Figure 19 corresponding to configuration B1.

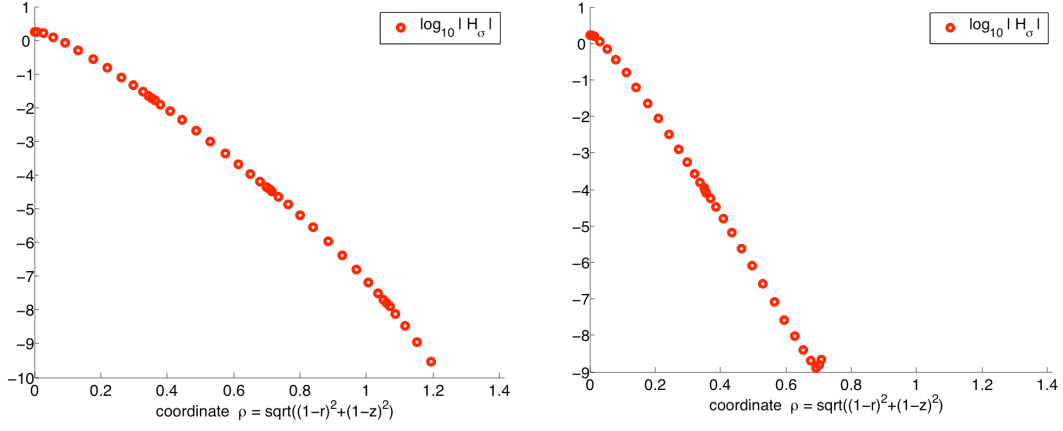


FIGURE 21. In circles, extracted values of $\log_{10} |\tilde{h}_\sigma(\rho)|$, ρ is the distance to the corner. On the left $\sigma = 20$ (interpolation degree $p = 12$). On the right, $\sigma = 80$ (degree $p = 16$). Configuration A

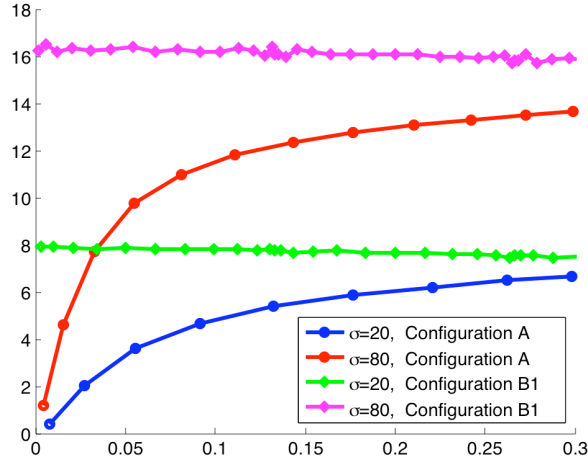


FIGURE 22. The graphs of the slopes $\tilde{s}_i(\sigma)$. Configuration A and B1, and $\sigma = 20$ (interpolation degree $p = 12$), $\sigma = 80$ (degree $p = 16$)

Whereas in configuration B1, the slopes clearly converge to a positive limit value as $\rho = y_3$ tends to 0, in configuration A the slopes tend to 0, which means that, *stricto sensu*, there is no exponential decay near the corner. Nevertheless we notice that in a region which is further away from the corner, a sort of exponential convergence is restored. This phenomenon is due to the fact that the principal asymptotic contribution inside the conductor is a *profile globally defined on an infinite sector* \mathcal{S} (of opening $\frac{\pi}{2}$ in the present

case) solving, instead the 1D problem (4.9) the model Dirichlet problem

$$(7.2) \quad \begin{cases} (\partial_X^2 + \partial_Y^2) \mathfrak{h}_0^\theta - \lambda^2 \mathfrak{h}_0^\theta &= 0 & \text{in } \mathcal{S}, \\ \mathfrak{h}_0^\theta &= \mathfrak{h}_0^+(\mathbf{a}) & \text{on } \partial\mathcal{S}. \end{cases}$$

8. CONCLUSION

Even though addressing axisymmetric configurations for which the Maxwell system can be reduced to one scalar equation, our numerical experiments are in significative accordance with our theoretical results concerning the decay of solutions inside the conductor and their structure in the skin layer. Our asymptotics provide an *a priori* knowledge on solutions, which can be used for the design of meshes in view of a good quality finite element approximation: The mesh should fit the boundary of the conductor and can be coarse far from its boundary inside the conductor – depending on the skin depth. In this perspective, it is interesting to compare with [16] where an adaptive *a posteriori* approach based on the *hp* method has been used for an industrial axisymmetric problem in electromagnetism.

APPENDIX A. ELEMENTS OF PROOF FOR THE MULTISCALE EXPANSION

Subsequently, we assume Assumption 2.1 on ω and Assumption 2.3 on the domains. In this framework, Theorem 2.2 gives the existence of δ_0 such that for all $\delta \leq \delta_0$, the problem (2.1)-(2.2) has a unique solution $(\mathbf{E}_{(\delta)}, \mathbf{H}_{(\delta)})$ which is denoted by $(\mathbf{E}_{(\delta)}^+, \mathbf{H}_{(\delta)}^+)$ in the dielectric part Ω_+ , and $(\mathbf{E}_{(\delta)}^-, \mathbf{H}_{(\delta)}^-)$ in the conducting part Ω_- . Furthermore, we suppose that the right hand side $\mathbf{j} \in \mathbf{H}_0(\text{div}, \Omega)$ is smooth and its support does not meet the conductor domain Ω_- .

Recall that (y_α, y_3) is a local *normal coordinate system* to the surface Σ in \mathcal{U}_- , see Figure 2. The function $\mathbf{y} \mapsto \chi(y_3)$ is a smooth cut-off with support in $\overline{\mathcal{U}}_-$ and equal to 1 in a smaller tubular neighborhood of Σ .

Theorem A.1. *Under the above assumptions, the solution $(\mathbf{E}_{(\delta)}, \mathbf{H}_{(\delta)})$ possesses the asymptotic expansion (see subsection A.7 below for precise estimates):*

$$(A.1) \quad \mathbf{E}_{(\delta)}^+(\mathbf{x}) \approx \sum_{j \geq 0} \delta^j \mathbf{E}_j^+(\mathbf{x}) \quad \text{and} \quad \mathbf{H}_{(\delta)}^+(\mathbf{x}) \approx \sum_{j \geq 0} \delta^j \mathbf{H}_j^+(\mathbf{x}),$$

$$(A.2) \quad \mathbf{E}_{(\delta)}^-(\mathbf{x}) \approx \sum_{j \geq 0} \delta^j \mathbf{E}_j^-(\mathbf{x}; \delta) \quad \text{with} \quad \mathbf{E}_j^-(\mathbf{x}; \delta) = \chi(y_3) \mathfrak{E}_j(y_\beta, \frac{y_3}{\delta}),$$

$$(A.3) \quad \mathbf{H}_{(\delta)}^-(\mathbf{x}) \approx \sum_{j \geq 0} \delta^j \mathbf{H}_j^-(\mathbf{x}; \delta) \quad \text{with} \quad \mathbf{H}_j^-(\mathbf{x}; \delta) = \chi(y_3) \mathfrak{H}_j(y_\beta, \frac{y_3}{\delta}),$$

where $\mathfrak{E}_j(y_\beta, \frac{y_3}{\delta}) \rightarrow 0$ and $\mathfrak{H}_j(y_\beta, \frac{y_3}{\delta}) \rightarrow 0$ when $\frac{y_3}{\delta} \rightarrow \infty$. Moreover, for any $j \in \mathbb{N}$, there holds

$$(A.4) \quad \mathbf{E}_j^+, \mathbf{H}_j^+ \in \mathbf{H}(\text{curl}, \Omega_+) \quad \text{and} \quad \mathfrak{E}_j, \mathfrak{H}_j \in \mathbf{H}(\text{curl}, \Sigma \times \mathbb{R}_+).$$

Hereafter, we present elements of proof of this theorem and details about the terms in asymptotics (A.2)–(A.3). In §A.1, we expand the “magnetic” Maxwell operators in power series of δ inside the boundary layer \mathcal{U}_- . We deduce in §A.2 the equations satisfied by the magnetic profiles, and derive explicitly the first ones in §A.3. Then in §A.4 and §A.5, we do the same for the electric profiles. As an alternative, we show how to deduce directly the magnetic profiles from the electrical ones in §A.6. In §A.7, we conclude to the validation of the asymptotic expansion with a convergence result.

A.1. Expansion of the operators. Integrating by parts in the magnetic variational formulation (2.7), we find the following Maxwell transmission problem

$$(A.5) \quad \begin{cases} \operatorname{curl} \operatorname{curl} \mathbf{H}_{(\delta)}^+ - \kappa^2 \mathbf{H}_{(\delta)}^+ = \operatorname{curl} \mathbf{j} & \text{in } \Omega_+ \\ \operatorname{curl} \operatorname{curl} \mathbf{H}_{(\delta)}^- - \kappa^2 (1 + \frac{i}{\delta^2}) \mathbf{H}_{(\delta)}^- = 0 & \text{in } \Omega_- \\ \operatorname{curl} \mathbf{H}_{(\delta)}^+ \times \mathbf{n} = (1 + \frac{i}{\delta^2})^{-1} \operatorname{curl} \mathbf{H}_{(\delta)}^- \times \mathbf{n} & \text{on } \Sigma \\ \mathbf{H}_{(\delta)}^+ \times \mathbf{n} = \mathbf{H}_{(\delta)}^- \times \mathbf{n} & \text{on } \Sigma \\ \mathbf{H}_{(\delta)}^+ \times \mathbf{n} = 0 & \text{on } \Gamma. \end{cases}$$

It is important to notice that, since $\kappa \neq 0$, it is a consequence of the above equations that

$$\operatorname{div} \mathbf{H}_{(\delta)} = 0 \quad \text{in } \Omega.$$

Therefore, we have in particular the extra transmission condition

$$(A.6) \quad \mathbf{H}_{(\delta)}^+ \cdot \mathbf{n} = \mathbf{H}_{(\delta)}^- \cdot \mathbf{n} \quad \text{on } \Sigma.$$

We denote by $\mathbf{L}(y_\alpha, h; D_\alpha, \partial_3^h)$ the 2d order Maxwell operator $\operatorname{curl} \operatorname{curl} - \kappa^2 (1 + \frac{i}{\delta^2}) \mathbb{I}$ set in \mathcal{U}_- in a *normal coordinate system*. Here D_α is the covariant derivative on the interface Σ , and ∂_3^h is the partial derivative with respect to the normal coordinate $y_3 = h$.

Let $a_{\alpha\beta}(h)$ be the metric tensor of the manifold Σ_h , which is the surface contained in Ω_- at a distance h of Σ , see Figure 2. According to [4, 6], the metric tensor in such a coordinate system writes

$$(A.7) \quad a_{\alpha\beta}(h) = a_{\alpha\beta} - 2b_{\alpha\beta}h + b_\alpha^\gamma b_{\gamma\beta}h^2,$$

and its inverse expands in power series of h

$$a^{\alpha\beta}(h) = a^{\alpha\beta} + 2b^{\alpha\beta}h + \mathcal{O}(h^2).$$

With this metric, a three-dimensional vector field \mathfrak{H} can be split into its normal component \mathfrak{h} and its tangential component that can be alternatively viewed as a vector field \mathfrak{H}^α or a one-form field \mathfrak{H}_α with the relation

$$(A.8) \quad \mathfrak{H}^\alpha = a^{\alpha\beta}(h) \mathfrak{H}_\beta.$$

Subsequently, we use a property of the covariant derivative, that it acts on functions like the partial derivative: $D_\alpha \mathfrak{h} = \partial_\alpha \mathfrak{h}$.

We denote by $\mathbf{T}(y_\alpha, h; D_\alpha, \partial_3^h)$ the tangent trace operator $(1 + \frac{i}{\delta^2})^{-1} \operatorname{curl} \cdot \times \mathbf{n}$ on Σ . If $\mathfrak{H} = (\mathfrak{H}_\alpha, \mathfrak{h})$, then

$$(A.9) \quad \mathbf{T}(y_\alpha, h; D_\alpha, \partial_3^h) \mathfrak{H} = (1 + \frac{i}{\delta^2})^{-1} (\partial_3^h \mathfrak{H}_\alpha - D_\alpha \mathfrak{h}) dy^\alpha,$$

see [17, Ch. 6, eq. (6.87)]. The operators \mathbf{L} and \mathbf{T} expand in power series of h with intrinsic coefficients with respect to Σ , see [6] for the 3D elasticity operator on a thin shell. We make the scaling $Y_3 = \delta^{-1}h$ to describe the boundary layer with respect to δ . Then, the three-dimensional harmonic Maxwell operators in \mathcal{U}_- are written $\mathbf{L}[\delta]$ and $\mathbf{T}[\delta]$. These operators expand in power series of δ with coefficients intrinsic operators :

$$\mathbf{L}[\delta] = \delta^{-2} \sum_{n=0}^{\infty} \delta^n \mathbf{L}^n \quad \text{and} \quad \mathbf{T}[\delta] = \sum_{n=1}^{\infty} \delta^n \mathbf{T}^n .$$

We denote by L_α^n and T_α^n the surface components of \mathbf{L}^n and \mathbf{T}^n . With the summation convention of repeated two dimensional indices (represented by greek letters), there holds

$$(A.10) \quad L_\alpha^0(\underline{\mathfrak{H}}) = -\partial_3^2 \mathfrak{H}_\alpha - i\kappa^2 \mathfrak{H}_\alpha \quad \text{and} \quad L_\alpha^1(\underline{\mathfrak{H}}) = -2b_\alpha^\beta \partial_3 \mathfrak{H}_\beta + \partial_3 D_\alpha \mathfrak{h} + b_\beta^\beta \partial_3 \mathfrak{H}_\alpha ,$$

and

$$(A.11) \quad T_\alpha^n(\underline{\mathfrak{H}}) = \begin{cases} (-i)^p \partial_3 \mathfrak{H}_\alpha & \text{if } n = 2p - 1 \\ i^p \partial_\alpha \mathfrak{h} & \text{if } n = 2p . \end{cases}$$

Here, ∂_3 is the partial derivative with respect to Y_3 . We denote by L_3^n the transverse components of \mathbf{L}^n . There holds

$$(A.12) \quad L_3^0(\underline{\mathfrak{H}}) = -i\kappa^2 \mathfrak{h} \quad \text{and} \quad L_3^1(\underline{\mathfrak{H}}) = \gamma_\alpha^\alpha (\partial_3 \underline{\mathfrak{H}}) + b_\beta^\beta \partial_3 \mathfrak{h} ,$$

where $\gamma_{\alpha\beta}(\underline{\mathfrak{H}}) = \frac{1}{2}(D_\alpha \mathfrak{H}_\beta + D_\beta \mathfrak{H}_\alpha) - b_{\alpha\beta} \mathfrak{h}$ is the change of metric tensor.

A.2. Equations for the coefficients of the magnetic field. The profiles $\underline{\mathfrak{H}}_j$ and the coefficients \mathbf{H}_j^+ of the magnetic field satisfy the following system

$$(A.13) \quad \mathbf{L}[\delta] \sum_{j \geq 0} \delta^j \underline{\mathfrak{H}}_j(y_\alpha, Y_3) = 0 \quad \text{in } \Sigma \times I ,$$

$$(A.14) \quad \mathbf{T}[\delta] \sum_{j \geq 0} \delta^j \underline{\mathfrak{H}}_j(y_\alpha, 0) = \sum_{j \geq 0} \delta^j \text{curl } \mathbf{H}_j^+ \times \mathbf{n} \quad \text{on } \Sigma ,$$

where $I = (0, +\infty)$. We perform in (A.13)-(A.14) the identification of terms with the same power in δ . The components of equation (A.13) are the collections of equations

$$(A.15) \quad \mathbf{L}^0(\underline{\mathfrak{H}}_0) = 0 , \quad \mathbf{L}^0(\underline{\mathfrak{H}}_1) + \mathbf{L}^1(\underline{\mathfrak{H}}_0) = 0 , \quad \text{and} \quad \sum_{l=0}^n \mathbf{L}^{n-l}(\underline{\mathfrak{H}}_l) = 0 ,$$

for all $n \geq 2$. Similarly, the surface components of the equation (A.14) write

$$(A.16) \quad \text{curl } \mathbf{H}_0^+ \times \mathbf{n} = 0 , \quad \text{and} \quad \sum_{k=1}^n \mathbf{T}^k \underline{\mathfrak{H}}_{n-k} = \text{curl } \mathbf{H}_n^+ \times \mathbf{n} ,$$

for all $n \geq 1$. Using the expression of the operator \mathbf{L}^0 , and expanding $\mathbf{H}_{(\delta)}^+$ in Ω_+ , we thus see that, according to the system (A.5), the profiles $\underline{\mathfrak{H}}_n = (\mathfrak{H}_n, \mathfrak{h}_n)$ and the terms

\mathbf{H}_n^+ have to satisfy, for all $n \geq 0$,

$$(A.17) \quad \left\{ \begin{array}{ll} (i) & -\lambda^2 \mathfrak{h}_n = \sum_{j=0}^{n-1} L_3^{n-j}(\underline{\mathfrak{H}}_j) \quad \text{in } \Sigma \times I \\ (ii) & \text{curl curl } \mathbf{H}_n^+ - \kappa^2 \mathbf{H}_n^+ = \delta_n^0 \text{curl } \mathbf{j} \quad \text{in } \Omega_+ \\ (iii) & \text{curl } \mathbf{H}_n^+ \times \mathbf{n} = \sum_{j=0}^{n-1} \mathbf{T}^{n-j} \underline{\mathfrak{H}}_j \quad \text{on } \Sigma \\ (iv) & \mathbf{H}_n^+ \times \mathbf{n} = 0 \quad \text{on } \Gamma \\ (v) & \partial_3^2 \mathfrak{H}_{n,\alpha} - \lambda^2 \mathfrak{H}_{n,\alpha} = \sum_{j=0}^{n-1} L_\alpha^{n-j}(\underline{\mathfrak{H}}_j) \quad \text{in } \Sigma \times I \\ (vi) & \mathfrak{H}_n = \mathbf{n} \times \mathbf{h}_n \times \mathbf{n} \quad \text{on } \Sigma. \end{array} \right.$$

where $\lambda = \kappa e^{-i\pi/4}$, cf (3.5) (so that $-\lambda^2 = i\kappa^2$) and \mathbf{h}_n denotes the trace of \mathbf{H}_n^+ on Σ . In (A.17), we use the convention that the sums are 0 when $n = 0$. The transmission condition (A.6) implies the extra continuity condition

$$(A.18) \quad \mathbf{H}_n^+ \cdot \mathbf{n} = \mathfrak{h}_n \quad \text{on } \Sigma.$$

The set of equations (A.17)–(A.18) allows to determine $\underline{\mathfrak{H}}_n$ and \mathbf{H}_n^+ by induction.

A.3. First terms of the magnetic field asymptotics. According to equation (i) in (A.17), the normal component \mathfrak{h}_0 of the first profile in the conductor vanishes:

$$(A.19) \quad \mathfrak{h}_0 = 0,$$

because $\kappa \neq 0$, thus $\lambda \neq 0$.

Hence, according to (A.17) (ii)–(iv) and (A.18), the first term of the magnetic field in the dielectric region solves Maxwell equations with perfectly conducting conditions on Σ :

$$(A.20) \quad \left\{ \begin{array}{ll} \text{curl curl } \mathbf{H}_0^+ - \kappa^2 \mathbf{H}_0^+ = \text{curl } \mathbf{j} & \text{in } \Omega_+ \\ \mathbf{H}_0^+ \cdot \mathbf{n} = 0 \quad \text{and} \quad \text{curl } \mathbf{H}_0^+ \times \mathbf{n} = 0 & \text{on } \Sigma \\ \mathbf{H}_0^+ \times \mathbf{n} = 0 & \text{on } \Gamma. \end{array} \right.$$

Thus the trace \mathbf{h}_0 of \mathbf{H}_0^+ on the interface Σ is *tangential*.

According to equations (v)–(vi) in (A.17), \mathfrak{H}_0 satisfies the following ODE

$$(A.21) \quad \left\{ \begin{array}{ll} \partial_3^2 \mathfrak{H}_0(\cdot, Y_3) - \lambda^2 \mathfrak{H}_0(\cdot, Y_3) = 0 & \text{for } Y_3 \in I = (0, \infty) \\ \mathfrak{H}_0(\cdot, 0) = (\mathbf{n} \times \mathbf{h}_0) \times \mathbf{n}. \end{array} \right.$$

The unique solution of (A.21) such that $\mathfrak{H}_0 \rightarrow 0$ when $Y_3 \rightarrow \infty$, is, with the choice (3.5) for λ , the tangential field $\mathfrak{H}_0(y_\beta, Y_3) = \mathbf{h}_0(y_\beta) e^{-\lambda Y_3}$. Combining with (A.19), we find that the first profile in the conductor region is exponential with the complex rate λ :

$$(A.22) \quad \underline{\mathfrak{H}}_0(y_\beta, Y_3) = \mathbf{h}_0(y_\beta) e^{-\lambda Y_3}.$$

The next term which is determined in the asymptotics is the normal component \mathfrak{h}_1 of the profile \mathfrak{H}_1 given by equation (i) of (A.17) for $n = 1$. We obtain

$$(A.23) \quad \mathfrak{h}_1(y_\beta, Y_3) = \lambda^{-1} D_\alpha h_0^\alpha(y_\beta) e^{-\lambda Y_3}.$$

According to (A.17) (ii)-(iv) and (A.18), the next term in the dielectric region solves:

$$(A.24) \quad \begin{cases} \operatorname{curl} \operatorname{curl} \mathbf{H}_1^+ - \kappa^2 \mathbf{H}_1^+ = 0 & \text{in } \Omega_+ \\ \mathbf{H}_1^+ \cdot \mathbf{n} = \mathfrak{h}_1 \quad \text{and} \quad \operatorname{curl} \mathbf{H}_1^+ \times \mathbf{n} = i\lambda \mathbf{h}_0 & \text{on } \Sigma \\ \mathbf{H}_1^+ \times \mathbf{n} = 0 & \text{on } \Gamma. \end{cases}$$

Recall that \mathbf{h}_1 is the trace of \mathbf{H}_1^+ on the interface Σ . We denote by $h_{1,\alpha}$ its tangential components. According to equations (v)-(vi) in (A.17) for $n = 1$, \mathfrak{H}_1 satisfies the following ODE (for $Y_3 \in I$)

$$(A.25) \quad \begin{cases} \partial_3^2 \mathfrak{H}_{1,\alpha}(\cdot, Y_3) - \lambda^2 \mathfrak{H}_{1,\alpha}(\cdot, Y_3) = -2b_\alpha^\sigma \partial_3 \mathfrak{H}_{0,\sigma}(\cdot, Y_3) + b_\beta^\beta \partial_3 \mathfrak{H}_{0,\alpha}(\cdot, Y_3) \\ \mathfrak{H}_{1,\alpha}(\cdot, 0) = h_{1,\alpha}(\cdot, 0). \end{cases}$$

From (A.22), the unique solution of (A.25) such that $\mathfrak{H}_1 \rightarrow 0$ when $Y_3 \rightarrow \infty$ is the profile

$$(A.26) \quad \mathfrak{H}_{1,\alpha}(y_\beta, Y_3) = \left[h_{1,\alpha} + Y_3 (H h_{0,\alpha} - b_\alpha^\sigma h_{0,\sigma}) \right] (y_\beta) e^{-\lambda Y_3}, \quad \alpha = 1, 2.$$

Using the relation (A.8) and performing the scaling $h = \delta Y_3$ in the previous equation, we obtain for the contravariant components

$$\mathfrak{H}_1^\alpha = a^{\alpha\beta} \mathfrak{H}_{1,\beta} + 2Y_3 b^{\alpha\beta} \mathfrak{H}_{0,\beta}.$$

From (A.22), and (A.26), the tangential components \mathfrak{H}_1^α are given by (3.9)

$$\mathfrak{H}_1^\alpha(y_\beta, Y_3) = \left[h_1^\alpha + Y_3 (H h_0^\alpha + b_\sigma^\alpha h_0^\sigma) \right] (y_\beta) e^{-\lambda Y_3}, \quad \alpha = 1, 2.$$

Remark A.2. Note that the boundary value problems (A.20) and (A.24) are well-posed. It is a consequence of the spectral Assumption 2.1 on ω .

A.4. Equations for the coefficients of the electric field. The second order Maxwell operator for the electric field writes

$$(A.27) \quad \begin{cases} \operatorname{curl} \operatorname{curl} \mathbf{E}_{(\delta)}^+ - \kappa^2 \mathbf{E}_{(\delta)}^+ = i\omega\mu_0 \mathbf{j} & \text{in } \Omega_+ \\ \operatorname{curl} \operatorname{curl} \mathbf{E}_{(\delta)}^- - \kappa^2 (1 + \frac{i}{\delta^2}) \mathbf{E}_{(\delta)}^- = 0 & \text{in } \Omega_- \\ \operatorname{curl} \mathbf{E}_{(\delta)}^+ \times \mathbf{n} = \operatorname{curl} \mathbf{E}_{(\delta)}^- \times \mathbf{n} & \text{on } \Sigma \\ \mathbf{E}_{(\delta)}^+ \times \mathbf{n} = \mathbf{E}_{(\delta)}^- \times \mathbf{n} & \text{on } \Sigma \\ \mathbf{E}_{(\delta)}^+ \cdot \mathbf{n} = 0 \quad \text{and} \quad \operatorname{curl} \mathbf{E}_{(\delta)}^+ \times \mathbf{n} = 0 & \text{on } \Gamma. \end{cases}$$

We denote by $\mathbf{B}(y_\alpha, h; D_\alpha, \partial_3^h)$ the tangent trace operator $\operatorname{curl} \cdot \times \mathbf{n}$ on Σ in a *normal coordinate system*. If $\mathfrak{E} = (\mathfrak{E}_\alpha, \mathfrak{e})$, then

$$(\mathbf{B}(y_\alpha, h; D_\alpha, \partial_3^h) \mathfrak{E})_\alpha = \partial_3^h \mathfrak{E}_\alpha - D_\alpha \mathfrak{e},$$

see [17, Ch. 3, Prop. 3.36]. We define $\mathbf{B}[\delta]$ the operator obtained from \mathbf{B} in \mathcal{U}_- after the scaling $Y_3 = \delta^{-1}h$. This operator expands in power of δ :

$$\mathbf{B}[\delta] = \delta^{-1}\mathbf{B}^0 + \mathbf{B}^1 .$$

Recall that ∂_3 is the partial derivative with respect to Y_3 . Thus, denoting by B_α^n the surface components of \mathbf{B}^n , we obtain

$$(A.28) \quad B_\alpha^0(\underline{\mathfrak{E}}) = \partial_3 \mathfrak{E}_\alpha \quad \text{and} \quad B_\alpha^1(\underline{\mathfrak{E}}) = -D_\alpha \mathfrak{e} .$$

According to the second and third equations in system (A.27), the profiles $\underline{\mathfrak{E}}_j$ and the terms \mathbf{E}_j^+ of the electric field satisfy the following system

$$(A.29) \quad \mathbf{L}[\delta] \sum_{j \geq 0} \delta^j \underline{\mathfrak{E}}_j(y_\alpha, Y_3) = 0, \quad \text{in} \quad \Sigma \times I ,$$

$$(A.30) \quad \mathbf{B}[\delta] \sum_{j \geq 0} \delta^j \underline{\mathfrak{E}}_j(y_\alpha, 0) = \sum_{j \geq 0} \delta^j \operatorname{curl} \mathbf{E}_j^+ \times \mathbf{n} \quad \text{on} \quad \Sigma .$$

We identify in (A.29)-(A.30) the terms with the same power in δ . The components of the equation (A.29) are collections of equations, similar to the equations (A.15) set for the magnetic field. The surface components of the equation (A.30) write

$$(A.31) \quad B_\alpha^0(\underline{\mathfrak{E}}_0) = 0, \quad \text{and} \quad B_\alpha^0(\underline{\mathfrak{E}}_{n+1}) + B_\alpha^1(\underline{\mathfrak{E}}_n) = (\operatorname{curl} \mathbf{E}_n^+ \times \mathbf{n})_\alpha ,$$

for all $n \geq 0$.

According to the system (A.27) and (A.28), the profiles $\underline{\mathfrak{E}}_n = (\mathfrak{E}_n, \mathfrak{e}_n)$ and the terms \mathbf{E}_n^+ have to satisfy, for all $n \geq 0$, (we recall $\lambda = \kappa e^{-i\pi/4}$, cf (3.5), so that $-\lambda^2 = i\kappa^2$)

$$(A.32) \quad \left\{ \begin{array}{ll} (i) & \partial_3^2 \mathfrak{E}_{n,\alpha} - \lambda^2 \mathfrak{E}_{n,\alpha} = \sum_{j=0}^{n-1} L_\alpha^{n-j}(\underline{\mathfrak{E}}_j) \quad \text{in} \quad \Sigma \times I \\ (ii) & \partial_3 \mathfrak{E}_{n,\alpha} = D_\alpha \mathfrak{e}_{n-1} + (\operatorname{curl} \mathbf{E}_{n-1}^+ \times \mathbf{n})_\alpha \quad \text{on} \quad \Sigma \\ (iii) & -\lambda^2 \mathfrak{e}_n = \sum_{j=0}^{n-1} L_3^{n-j}(\underline{\mathfrak{E}}_j) \quad \text{in} \quad \Sigma \times I \\ (iv) & \operatorname{curl} \operatorname{curl} \mathbf{E}_n^+ - \kappa^2 \mathbf{E}_n^+ = \delta_n^0 i\omega \mu_0 \mathbf{j} \quad \text{in} \quad \Omega_+ \\ (v) & \mathbf{E}_n^+ \times \mathbf{n} = \mathfrak{E}_n \times \mathbf{n} \quad \text{on} \quad \Sigma \\ (vi) & \mathbf{E}_n^+ \cdot \mathbf{n} = 0 \quad \text{and} \quad \operatorname{curl} \mathbf{E}_n^+ \times \mathbf{n} = 0 \quad \text{on} \quad \Gamma. \end{array} \right.$$

Hereafter, we determine the terms $\underline{\mathfrak{E}}_n$ and \mathbf{E}_n^+ by induction.

A.5. First terms of the asymptotics for the electric field. According to equations (i)-(ii) in system (A.32) for $n = 0$, $\underline{\mathfrak{E}}_0$ satisfies the following ODE

$$(A.33) \quad \begin{cases} \partial_3^2 \mathfrak{E}_0(\cdot, Y_3) - \lambda^2 \mathfrak{E}_0(\cdot, Y_3) = 0 & \text{for } Y_3 \in I, \\ \partial_3 \mathfrak{E}_0(\cdot, 0) = 0. \end{cases}$$

The unique solution of (A.33) such that $\mathfrak{E}_0 \rightarrow 0$ when $Y_3 \rightarrow \infty$, is $\mathfrak{E}_0 = 0$. From equation (iii) in system (A.32) for $n = 0$, there holds $\mathfrak{e}_0 = 0$. We infer

$$(A.34) \quad \underline{\mathfrak{E}}_0(y_\beta, Y_3) = 0 .$$

From equations (iv)-(vi) in (A.32) for $n = 0$, and from (A.34), the first asymptotic of the electric field in the dielectric part solves the following problem

$$\begin{cases} \operatorname{curl} \operatorname{curl} \mathbf{E}_0^+ - \kappa^2 \mathbf{E}_0^+ = i\omega\mu_0 \mathbf{j} & \text{in } \Omega_+ \\ \mathbf{E}_0^+ \times \mathbf{n} = 0 & \text{on } \Sigma \\ \mathbf{E}_0^+ \cdot \mathbf{n} = 0 \quad \text{and} \quad \operatorname{curl} \mathbf{E}_0^+ \times \mathbf{n} = 0 & \text{on } \Gamma. \end{cases}$$

According to the spectral Assumption 2.1, this boundary value problem is well-posed.

The next term determined in the asymptotic expansion is \mathfrak{E}_1 . From equations (i)-(ii) in (A.32) for $n = 1$, \mathfrak{E}_1 satisfies for $Y_3 \in I$

$$\begin{cases} \partial_3^2 \mathfrak{E}_1(\cdot, Y_3) - \lambda^2 \mathfrak{E}_1(\cdot, Y_3) = 0 \\ \partial_3 \mathfrak{E}_1(\cdot, 0) = (\operatorname{curl} \mathbf{E}_0^+ \times \mathbf{n})(\cdot, 0). \end{cases}$$

We denote by $\mathbf{j}_k(y_\beta) = \lambda^{-1}(\operatorname{curl} \mathbf{E}_k^+ \times \mathbf{n})(y_\beta, 0)$ for $k = 0, 1$. Hence,

$$(A.35) \quad \mathfrak{E}_1(y_\beta, Y_3) = -\mathbf{j}_0(y_\beta) e^{-\lambda Y_3}.$$

From equation (iii) in (A.32) for $n = 1$, and from (A.34), we obtain $\mathfrak{e}_1 = 0$. From equations (iv)-(vi) in (A.32) for $n = 1$, and from (A.35), the asymptotic of order 1 for the electric field in the dielectric part solves :

$$\begin{cases} \operatorname{curl} \operatorname{curl} \mathbf{E}_1^+ - \kappa^2 \mathbf{E}_1^+ = 0 & \text{in } \Omega_+ \\ \mathbf{E}_1^+ \times \mathbf{n} = -\mathbf{j}_0 \times \mathbf{n} & \text{on } \Sigma \\ \mathbf{E}_1^+ \cdot \mathbf{n} = 0 \quad \text{and} \quad \operatorname{curl} \mathbf{E}_1^+ \times \mathbf{n} = 0 & \text{on } \Gamma. \end{cases}$$

Then, from equations (i)-(ii) in (A.32) for $n = 2$, $\mathfrak{E}_{2,\alpha}$ solves the ODE for $Y_3 \in I$:

$$\begin{cases} \partial_3^2 \mathfrak{E}_{2,\alpha}(\cdot, Y_3) - \lambda^2 \mathfrak{E}_{2,\alpha}(\cdot, Y_3) = -2b_\alpha^\sigma \partial_3 \mathfrak{E}_{1,\sigma}(\cdot, Y_3) + b_\beta^\beta \partial_3 \mathfrak{E}_{1,\alpha}(\cdot, Y_3) \\ \partial_3 \mathfrak{E}_{2,\alpha}(\cdot, 0) = (\operatorname{curl} \mathbf{E}_1^+ \times \mathbf{n})_\alpha(\cdot, 0). \end{cases}$$

We denote by $\mathbf{j}_{k,\alpha}$ the surface components of \mathbf{j}_k , for $k = 0, 1$. We obtain

$$(A.36) \quad \mathfrak{E}_{2,\alpha}(y_\beta, Y_3) = \left[-\mathbf{j}_{1,\alpha} + (\lambda^{-1} + Y_3)(b_\alpha^\sigma \mathbf{j}_{0,\sigma} - H \mathbf{j}_{0,\alpha}) \right] (y_\beta) e^{-\lambda Y_3}.$$

From equation (iii) in (A.32) for $n = 2$, we infer

$$\mathfrak{e}_2(y_\beta, Y_3) = -\lambda^{-1} D_\alpha \mathbf{j}_0^\alpha(y_\beta) e^{-\lambda Y_3}.$$

A.6. From \mathbf{E} to \mathbf{H} in the conducting part. An alternative way of calculating the magnetic profiles is to deduce them from the electric ones by means of a *normal parameterization* of the intrinsic curl operator, see [17, Ch. 3]. Let $\underline{\mathfrak{E}} = (\mathfrak{E}_\alpha, \mathfrak{e})$ be a 1-form fields in \mathcal{U}_- . There holds:

$$(A.37) \quad (\nabla \times \underline{\mathfrak{E}})^\alpha = \epsilon^{3\beta\alpha} (\partial_3^h \mathfrak{E}_\beta - \partial_\beta \mathfrak{e}) \quad \text{and} \quad (\nabla \times \underline{\mathfrak{E}})^3 = \epsilon^{3\alpha\beta} D_\alpha^h \mathfrak{E}_\beta \quad \text{on } \Sigma_h.$$

Here, D_α^h is the *covariant derivative* on Σ_h , and ϵ is the Levi-Civita tensor, see [10, 7]. The contravariant components ϵ^{ijk} of ϵ depend on the normal coordinate h , and write in a *normal coordinate* system

$$\epsilon^{ijk} = (\det a_{\alpha\beta}(h))^{-1/2} \epsilon_0(i, j, k).$$

Here, $a_{\alpha\beta}(h)$ is the metric tensor of the manifold Σ_h , see (A.7). The indices $i, j, k \in \{1, 2, 3\}$, and $\epsilon_0(i, j, k)$ equals 1 when (i, j, k) is an even circular permutation, and equals -1 when (i, j, k) is an odd circular permutation, and $\epsilon_0(i, j, k) = 0$ otherwise.

Remark A.3. Let $a = \det(a_{\alpha\beta})$, and recall that $b_\nu^\nu = 2H$. Then using (A.7) we obtain

$$\epsilon^{ijk} = a^{-1/2} (1 + 2Hh + O(h^2)) \epsilon_0(i, j, k).$$

We make the scaling $h = \delta Y_3$ and expand equations (A.37) in power series of δ :

$$(A.38) \quad (\nabla \times \underline{\mathfrak{E}})^\alpha = \delta^{-1} j^{\beta\alpha} \partial_3 \mathfrak{E}_\beta + j^{\beta\alpha} (2HY_3 \partial_3 \mathfrak{E}_\beta - \partial_\beta \mathfrak{e}) + \mathcal{O}(\delta),$$

$$(A.39) \quad (\nabla \times \underline{\mathfrak{E}})^3 = j^{\alpha\beta} D_\alpha \mathfrak{E}_\beta + \delta Y_3 j^{\alpha\beta} (2HD_\alpha \mathfrak{E}_\beta + \mathfrak{E}_\nu D_\alpha b_\beta^\nu) + \mathcal{O}(\delta^2).$$

Here,

$$j^{\alpha\beta} = a^{-1/2} \epsilon_0(\alpha, \beta, 3).$$

From the expansions (A.2) and (A.1) combined with Faraday's law (2.1) written in normal coordinates, we obtain the *profiles* $\underline{\mathfrak{H}}_j$ in the expansion (A.3) of the magnetic field from the profiles \mathfrak{E}_j of the electrical field. In particular, from (A.34), (A.35), and (A.36), we obtain explicitly the first terms $\underline{\mathfrak{H}}_0$ and $\underline{\mathfrak{H}}_1$, see (A.22), (3.9), and (A.23).

A.7. Convergence result. The validation of the asymptotic expansion (A.1), (A.2), (A.3), and (A.4), consists in proving estimates for remainders defined as

$$(A.40) \quad \mathbf{R}_{m;\delta}^{\mathbf{E}} = \mathbf{E}_{(\delta)} - \sum_{j=0}^m \delta^j \mathbf{E}_j \quad \text{and} \quad \mathbf{R}_{m;\delta}^{\mathbf{H}} = \mathbf{H}_{(\delta)} - \sum_{j=0}^m \delta^j \mathbf{H}_j \quad \text{in } \Omega.$$

By construction of the terms $\mathbf{E}_j = (\mathbf{E}_j^+, \mathbf{E}_j^-)$ in the dielectric and conductor parts, the remainders $\mathbf{R}_{m;\delta}^{\mathbf{E}}$ satisfy the assumption of [3, Th. 5.1], which is an estimate on the right hand side when the Maxwell operator is applied to $\mathbf{R}_{m;\delta}^{\mathbf{E}}$.

Thus [3, Th. 5.1] yields that for all $m \in \mathbb{N}$, and $\delta \in (0, \delta_0)$, there holds the optimal estimate

$$(A.41) \quad \|\mathbf{R}_{m;\delta}^{\mathbf{E},+}\|_{0,\Omega_+} + \|\operatorname{curl} \mathbf{R}_{m;\delta}^{\mathbf{E},+}\|_{0,\Omega_+} + \delta^{-\frac{1}{2}} \|\mathbf{R}_{m;\delta}^{\mathbf{E},-}\|_{0,\Omega_-} + \delta^{\frac{1}{2}} \|\operatorname{curl} \mathbf{R}_{m;\delta}^{\mathbf{E},-}\|_{0,\Omega_-} \leq C_m \delta^{m+1}.$$

Using Maxwell equations (2.1), we can deduce a similar estimate for $\mathbf{R}_{m;\delta}^{\mathbf{H}}$: We have

$$(A.42) \quad \mathbf{R}_{m;\delta}^{\mathbf{H},+} = (i\omega\mu_0)^{-1} \operatorname{curl} \mathbf{R}_{m;\delta}^{\mathbf{E},+} \quad \text{and} \quad \operatorname{curl} \mathbf{R}_{m;\delta}^{\mathbf{H},+} = (i\omega\mu_0)^{-1} \kappa^2 \mathbf{R}_{m;\delta}^{\mathbf{E},+}.$$

Hence, according to (A.41), we infer

$$\|\mathbf{R}_{m;\delta}^{\mathbf{H},+}\|_{0,\Omega_+} + \|\operatorname{curl} \mathbf{R}_{m;\delta}^{\mathbf{H},+}\|_{0,\Omega_+} \leq c_m \delta^{m+1}.$$

In Ω_- , the presence of profiles in the expansion prevents to link $\mathbf{R}_{m;\delta}^{\mathbf{H},-}$ and $\mathbf{R}_{m;\delta}^{\mathbf{E},-}$ via the Maxwell equations in a similar way as (A.42). Nevertheless, there holds also uniform estimates for $\mathbf{R}_{m;\delta}^{\mathbf{H},-}$:

$$\delta^{-\frac{1}{2}} \|\mathbf{R}_{m;\delta}^{\mathbf{H},-}\|_{0,\Omega_-} + \delta^{\frac{1}{2}} \|\operatorname{curl} \mathbf{R}_{m;\delta}^{\mathbf{H},-}\|_{0,\Omega_-} \leq C'_m \delta^{m+1}.$$

APPENDIX B. THE MULTISCALE EXPANSION OF THE ORTHORADIAL COMPONENT

We denote by $(\vec{e}_r, \vec{e}_\theta, \vec{e}_z)$ the basis associated with the cylindric coordinates (r, θ, z) .

B.1. Expansion of the operators. In the basis (\vec{e}_r, \vec{e}_z) , recall that $(r(\xi), z(\xi)) = \tau(\xi)$, $\xi \in (0, L)$ is an *arc-length coordinate* on the interface Σ^m , and $(\xi, h = y_3)$ is the associate normal coordinate system, see §4.2.2. The normal vector $\mathbf{n}(\xi)$ at the point $\tau(\xi)$ writes

$$\mathbf{n}(\xi) = (-z'(\xi), r'(\xi)) .$$

Hence, the tubular neighborhood \mathcal{U}_-^m of Σ^m inside Ω_-^m is represented thanks to the parameterization

$$\Psi : (\xi, h) \longmapsto (r, z) ,$$

$$(B.1) \quad \text{where } r = r(\xi) - h z'(\xi) , \quad \text{and } z = z(\xi) + h r'(\xi) .$$

Remark B.1. The curvature $k(\xi)$ at the point $\tau(\xi)$ is defined by

$$(B.2) \quad k(\xi) = (r' z'' - z' r'')(\xi) .$$

For $h_0 < 1/\|k\|_\infty$ the change of coordinates Ψ is a \mathcal{C}^∞ -diffeomorphism from the cylinder $\mathbb{T}_L \times [0, h_0)$ into \mathcal{U}_-^m :

$$\mathcal{U}_-^m = \Psi(\mathbb{T}_L \times [0, h_0)) .$$

Thanks to (B.1), we obtain

$$\begin{pmatrix} \partial_r \\ \partial_z \end{pmatrix} = (1 - h k(\xi))^{-1} \begin{pmatrix} r' & -(z' + h r'') \\ z' & (r' - h z'') \end{pmatrix} \begin{pmatrix} \partial_\xi \\ \partial_h \end{pmatrix} .$$

To perform the formal expansion of h_δ^- solution of (4.5) in Ω_-^m , we first use the change of variables Ψ in order to write the equations in the cylinder $\mathbb{T}_L \times [0, h_0)$. We then perform the rescaling

$$(B.3) \quad Y = \delta^{-1} h$$

in the equations set in Ω_-^m and Σ^m in order to make appear the small parameter δ in the equations. Actually δ appears in the equations set in Ω_- through the expression of the operator $(1 + \frac{i}{\delta^2})^{-1} D$, where D is defined by (4.7). We obtain the formal expansion:

$$D = \delta^{-2} [\partial_Y^2 + \delta D_1 + \delta^2 R_\delta] ,$$

where $D_1(\xi, Y; \partial_\xi, \partial_Y) = -(k(\xi) + \frac{z'}{r}(\xi)) \partial_Y$, and R_δ is an operator, which has smooth coefficients in ξ and Y , bounded in δ . Hence, we obtain

$$i(1 + \frac{i}{\delta^2})^{-1} D + \kappa^2 \mathbb{I} = A_0 + \delta A_1 + \delta^2 Q_\delta ,$$

with $A_0 = \partial_Y^2 - \lambda^2 \mathbb{I}$ and $A_1 = -(k + \frac{z'}{r})(\xi) \partial_Y$. Similarly, there holds

$$B = \delta^{-1} \partial_Y - \frac{z'}{r}(\xi)$$

on the interface Σ^m , and

$$(1 + \frac{i}{\delta^2})^{-1} \mathbf{B} = -i\delta\partial_Y + \delta^2 \mathbf{P}_\delta.$$

Note that these expansions correspond to the expansions (A.9) in orthoradial symmetry.

B.2. From the 3D asymptotic expansion to the 1D expansion. In this subsection, we show that we can obtain the profiles \mathfrak{h}_0^θ , and \mathfrak{h}_1^θ defined by (4.10) and (4.13) from the general profiles \mathfrak{H}_0^α and \mathfrak{H}_1^α defined above.

We set $(y_\alpha) := (\xi, \theta)$ a coordinate system on Σ . Thus, the *normal coordinate* system (y_α, h) on \mathcal{U}_- is induced by the *normal coordinate* system (ξ, h) on \mathcal{U}_-^m . The tubular neighborhood \mathcal{U}_- is parameterized by

$$\Phi : (y_\alpha, h) \mapsto (r \cos \theta, r \sin \theta, z),$$

where r and z are defined by (B.1). The associated tangent coordinate vector fields are

$$(B.4) \quad \mathbf{x}_1(h) = (r'(\xi) - h z''(\xi)) \vec{e}_r + (z'(\xi) + h r''(\xi)) \vec{e}_z,$$

$$(B.5) \quad \mathbf{x}_2(h) = (r(\xi) - h z'(\xi)) \vec{e}_\theta.$$

The normal coordinate vector field is $\mathbf{x}_3(h) = \mathbf{n}(\xi) = -z'(\xi) \vec{e}_r + r'(\xi) \vec{e}_z$.

A vector field $\underline{\mathfrak{H}} : (y_\alpha, h) \mapsto \underline{\mathfrak{H}}(y_\alpha, h)$ in \mathcal{U}_- writes (here $\alpha = 1, 2$)

$$\underline{\mathfrak{H}} = \mathfrak{H}^\alpha \mathbf{x}_\alpha(h) + \mathfrak{h}^\theta \mathbf{n},$$

and corresponds to the magnetic field in *cylindric* components

$$\check{\mathbf{H}}(r, \theta, z) = H_r(r, \theta, z) \vec{e}_r + H_\theta(r, \theta, z) \vec{e}_\theta + H_z(r, \theta, z) \vec{e}_z.$$

Using (B.5) we easily obtain

$$(r(\xi) - h z'(\xi)) \mathfrak{H}^2 = H_\theta,$$

and introducing the stretched variable $Y = \delta^{-1} h$, it follows

$$(B.6) \quad (r(\xi) - \delta Y z'(\xi)) \mathfrak{H}^2 = H_\theta.$$

We insert the following expansions

$$\mathfrak{H}^2 = \mathfrak{H}_0^2(y_\alpha, Y) + \delta \mathfrak{H}_1^2(y_\alpha, Y) + \mathcal{O}(\delta^2),$$

$$H_\theta = \mathfrak{h}_0^\theta(\xi, Y) + \delta \mathfrak{h}_1^\theta(\xi, Y) + \mathcal{O}(\delta^2)$$

in equation (B.6). Then we perform the identification of terms with the same power in δ . We obtain the equations

$$(B.7) \quad r(\xi) \mathfrak{H}_0^2 = \mathfrak{h}_0^\theta,$$

$$(B.8) \quad r(\xi) \mathfrak{H}_1^2 - Y z'(\xi) \mathfrak{H}_0^2 = \mathfrak{h}_1^\theta.$$

According to (A.22), and (3.9) for $\alpha = 2$, there holds

$$(B.9) \quad r(\xi) \mathfrak{H}_1^2 - Y z'(\xi) \mathfrak{H}_0^2 = r(\xi) \left[\mathfrak{h}_1^2 + Y (H \mathfrak{h}_0^2 + b_\sigma^2 \mathfrak{h}_0^\sigma - \frac{z'}{r} \mathfrak{h}_0^2) \right] e^{-\lambda Y}.$$

Lemma B.2. *The main curvatures κ_1, κ_2 of the interface Σ , and its mean curvature $H = \frac{1}{2}(\kappa_1 + \kappa_2)$ are*

$$\kappa_1 = k, \quad \kappa_2 = \frac{z'}{r}, \quad \text{and} \quad H = \frac{1}{2} \left(k + \frac{z'}{r} \right).$$

This result together with (B.9) yields

$$r(\xi) \mathfrak{H}_1^2 - Y z'(\xi) \mathfrak{H}_0^2 = r(\xi) \left[h_1^2 + \frac{Y}{2} \left(k + \frac{z'}{r} \right) (\xi) h_0^2 \right] e^{-\lambda Y}.$$

We set $r(\xi) h_j^2(y_\beta) = h_j^+(\tau(\xi))$, for $j = 0, 1$. Then, we infer (4.10)-(4.13) from the equations (A.22)-(3.9).

B.3. Proof of the lemma B.2. The *main curvatures* are defined by $\kappa_1 = b_1^1, \kappa_2 = b_2^2$, where $b_{\alpha\beta}$ is the curvature tensor. In this coordinate system on \mathcal{U}_- , the metric is defined by

$$g_{ij}(h) = \langle \mathbf{x}_i(h), \mathbf{x}_j(h) \rangle_{\mathbb{R}^3}.$$

From (B.4)-(B.5), we obtain

$$g_{ij}(h) = \begin{pmatrix} (r'(\xi) - h z''(\xi))^2 + (z'(\xi) + h r''(\xi))^2 & 0 & 0 \\ 0 & (r(\xi) - h z'(\xi))^2 & 0 \\ 0 & 0 & 1 \end{pmatrix}$$

Recall that

$$g_{\alpha\beta}(h) = a_{\alpha\beta} - 2b_{\alpha\beta}h + b_\alpha^\gamma b_{\gamma\beta}h^2.$$

Hence, the curvature tensor on the interface Σ is diagonal, and its diagonal components write

$$(B.10) \quad b_{11} = k \quad \text{and} \quad b_{22} = r z',$$

where $k = k(\xi)$ is defined by (B.2). The inverse of the metric tensor $a_{\alpha\beta}$ in Σ is diagonal and there holds

$$a^{11} = 1 \quad \text{and} \quad a^{22} = r^{-2}.$$

From (B.10), we deduce the lemma.

REFERENCES

- [1] C. Bernardi, M. Dauge, and Y. Maday. *Spectral methods for axisymmetric domains*, volume 3 of *Series in Applied Mathematics (Paris)*. Gauthier-Villars, Éditions Scientifiques et Médicales Elsevier, Paris, 1999. Numerical algorithms and tests due to Mejdi Azaïez.
- [2] P. Boisssoles. *Problèmes mathématiques et numériques issus de l'imagerie par résonance magnétique nucléaire*. PhD thesis, Université Rennes 1, 2005.
- [3] G. Caloz, M. Dauge, and V. Péron. Uniform estimates for transmission problems with high contrast in heat conduction and electromagnetism. *Journal of Mathematical Analysis and Applications*, 370(2):555–572, 2010.
- [4] M. Dauge, E. Faou, and V. Péron. Comportement asymptotique à haute conductivité de l'épaisseur de peau en électromagnétisme. *C. R. Acad. Sci. Paris Sér. I Math.*, 348(7-8):385–390, 2010.
- [5] M. Dauge, V. Péron, and C. Poignard. Asymptotic expansion for the solution of a stiff transmission problem in electromagnetism with a singular interface. (In preparation), 2010.
- [6] E. Faou. Elasticity on a thin shell: formal series solution. *Asymptot. Anal.*, 31(3-4):317–361, 2002.
- [7] H. Goldstein. *Classical mechanics*. Addison-Wesley Publishing Co., Reading, Mass., second edition, 1980. Addison-Wesley Series in Physics.
- [8] H. Haddar, P. Joly, and H.-M. Nguyen. Generalized impedance boundary conditions for scattering problems from strongly absorbing obstacles: the case of Maxwell's equations. *Math. Models Methods Appl. Sci.*, 18(10):1787–1827, 2008.
- [9] R. Hiptmair and P. D. Ledger. Computation of resonant modes for axisymmetric Maxwell cavities using hp -version edge finite elements. *Internat. J. Numer. Methods Engrg.*, 62(12):1652–1676, 2005.
- [10] T. Levi-Civita. *The absolute differential calculus*. Dover Phoenix Editions. Dover Publications Inc., Mineola, NY, 2005. Calculus of tensors, Translated from the Italian by Marjorie Long, Edited by Enrico Persico, Reprint of the 1926 translation.
- [11] R. C. MacCamy and E. Stephan. Solution procedures for three-dimensional eddy current problems. *J. Math. Anal. Appl.*, 101(2):348–379, 1984.
- [12] R. C. MacCamy and E. Stephan. A skin effect approximation for eddy current problems. *Arch. Rational Mech. Anal.*, 90(1):87–98, 1985.
- [13] D. Martin. Mélina, bibliothèque de calculs éléments finis. Source code. <http://anum-maths.univ-rennes1.fr/melina>, 1990-2010.
- [14] P.M. Naghdi. Foundations of elastic shell theory. In *Progress in Solid Mechanics, Vol. IV*, pages 1–90. North-Holland, Amsterdam, 1963.
- [15] B. Nkemzi. On the solution of Maxwell's equations in axisymmetric domains with edges. *ZAMM Z. Angew. Math. Mech.*, 85(8):571–592, 2005.
- [16] D. Pardo, L. Demkowicz, C. Torres-Verdín, and M. Paszynski. Two-dimensional high-accuracy simulation of resistivity logging-while-drilling (LWD) measurements using a self-adaptive goal-oriented hp finite element method. *SIAM J. Appl. Math.*, 66(6):2085–2106, 2006.
- [17] V. Péron. *Modélisation mathématique de phénomènes électromagnétiques dans des matériaux à fort contraste*. PhD thesis, Université Rennes 1, 2009. <http://tel.archives-ouvertes.fr/tel-00421736/fr/>.
- [18] S. M. Rytov. Calcul du skin effect par la méthode des perturbations. *Journal of Physics*, 11(3):233–242, 1940.
- [19] Christoph Schwab and Manil Suri. The p and hp versions of the finite element method for problems with boundary layers. *Math. Comp.*, 65(216):1403–1429, 1996.
- [20] E. Stephan. Solution procedures for interface problems in acoustics and electromagnetics. In *Theoretical acoustics and numerical techniques*, volume 277 of *CISM Courses and Lectures*, pages 291–348. Springer, Vienna, 1983.